Aerosol Science and Technology

ISSN: 0278-6826 (Print) 1521-7388 (Online) Journal homepage: http://www.tandfonline.com/loi/uast20

Modeling Source Contributions to Submicron Particle Number Concentrations Measured in Rochester, New York

David Ogulei , Philip K. Hopke , David C. Chalupa & Mark J. Utell

To cite this article: David Ogulei , Philip K. Hopke , David C. Chalupa & Mark J. Utell (2007) Modeling Source Contributions to Submicron Particle Number Concentrations Measured in Rochester, New York, Aerosol Science and Technology, 41:2, 179-201, DOI: 10.1080/02786820601116012

To link to this article: http://dx.doi.org/10.1080/02786820601116012

Published online: 17 Jan 2007.

Submit your article to this journal

Article views: 241

View related articles

Citing articles: 26 View citing articles

Full Terms & Conditions of access and use can be found at
http://www.tandfonline.com/action/journalInformation?journalCode=uast20

Download by: [University of North Texas] **Date:** 06 January 2017, At: 01:44

Aerosol Science and Technology, 41:179–201, 2007
Copyright © American Association for Aerosol Research
ISSN: 0278-6826 print / 1521-7388 online
DOI: 10.1080/02786820601116012

Modeling Source Contributions to Submicron Particle Number Concentrations Measured in Rochester, New York

David Ogulei,[1] Philip K. Hopke,[1] David C. Chalupa,[2] and Mark J. Utell[2]
[1]*Department of Chemical and Biomolecular Engineering, Clarkson University, Potsdam, NY, USA*
[2]*Department of Environmental Medicine, University of Rochester Medical Center, Rochester, NY, USA*

An advanced receptor model was used to elicit source information based on ambient submicron (0.01–0.47 μm) particle number concentrations, gaseous species, and meteorological variables measured at the New York State Department of Environmental Conservation central monitoring site in Rochester, NY. Four seasonal data sets (winter, spring, summer, and fall) were independently investigated. A total of ten different sources were identified, including two traffic factors, two nucleation factors, industrial emissions, residential/commercial heating, secondary nitrate, secondary sulfate, ozone-rich secondary aerosol, and regionally transported aerosol. The resolved sources were generally characterized by similar number modes for either winter, spring, summer or fall. The size distributions for nucleation were dominated by the smallest particles (<10–30 nm) that gradually grew to larger sizes as could be seen by observing the volume profiles. In addition, the nucleation factors were closely linked to traffic rush hours suggesting that cooling of tail-pipe emissions may have induced nucleation activity in the vicinity of the highways. Although the diurnal pattern of each of the two traffic factors closely followed traffic rush hour for Rochester, their size modes were different suggesting that these factors might represent local and remote emissions. Industrial emissions were dominated by emissions from coal-fired power plants that were located to the northwest of the sampling site. These facilities represent the largest point emission sources of SO_2, and probably ultrafine (<0.1 μm) or submicron particles, in Rochester. Regionally transported material was characterized by accumulation mode particles. Air parcel back-trajectories showed transport of air masses from the industrial midwest.

Received 12 March 2006; accepted 13 November 2006.
This work was supported by the United States Environmental Protection Agency (EPA) through Science to Achieve Results (STAR) grant RD83107801 and the New York State Energy Research and Development Authority (NYSERDA) through contract 8650. Although the research described in this article has been funded wholly or in part by the EPA, it has not been subjected to the Agency's required peer and policy review and therefore, does not necessarily reflect the views of the Agency and no official endorsement should be inferred. The authors gratefully acknowledge the NOAA Air Resources Laboratory (ARL) for the provision of the HYSPLIT transport and dispersion model used in this publication.
Address correspondence to Philip K. Hopke, Center for Air Resources Engineering and Science and Department of Chemical and Biomolecular Engineering, Clarkson University, PO. Box 5708, Potsdam, NY 13699-5708, USA. E-mail: hopkepk@clarkson.edu

INTRODUCTION

The health effects of ambient particulate matter have been studied by numerous investigators in the United States and other countries. However, most of these studies are based on particle mass and do not adequately address submicron particles, especially ultrafine (<0.1 μm) or sub-0.5 μm particles whose contribution to the total aerosol mass is comparably very small. There have been recent studies suggesting that the number of ultrafine particles (UFPs) may be as important as the total respirable mass (Seaton et al. 1995; Peters et al. 1997; Laden et al. 2000; Wichmann et al. 2000; Ibald-Mulli et al. 2002; Nygaard et al. 2004). UFPs can easily be inhaled and deposited in the respiratory tract thereby causing serious health effects (Oberdörster et al. 1995; Pekkanen et al. 1997). Inhaled ultrafine particles can be deposited in the lung and then migrate into systemic circulation and thus to the heart as well as to more distal organs (Penn et al. 2005). Toxic air pollutants carried by UFPs induce inflammatory responses through reactive oxygen species (ROS) or other mechanisms (Sioutas et al. 2005).

The present study examines size-resolved aerosol number concentrations of ultrafine (<0.1 μm) and sub-0.5 μm particles measured in a medium-sized urban airshed. The identification of sources of UFPs and sub-0.5 μm particles contributing to the observed particle number concentrations is important in any health effects study involving these particles. Different sources of such particles may elicit different health responses due to differences in the size distributions of particles emitted from those sources. Presently, very little information is available on the size distribution profiles of different sources of UFPs or sub-0.5 μm particles. This is partly because the majority of the present source apportionment studies are based on particle composition measurements and thus inadequately address the contributions from these particles.

In this study, the bilinear receptor model, two-way Positive Matrix Factorization (PMF2), is used to elicit source information based on ambient particle number concentrations, gaseous species, and meteorological variables measured in Rochester, NY. A number of authors have previously used this model to identify sources of fine particle mass (e.g., Lee et al. 1999; Song et al. 2001; Qin et al. 2002; Kim et al. 2003; Li et al. 2004;

Hien et al. 2004, 2005; Song et al. 2006). However, only very few efforts have utilized particle size measurements to identify sources of fine or ultrafine aerosol particles. Recently, PMF2 was employed to obtain source information based on ambient particle size distributions (Kim et al. 2004; Zhou et al. 2005a, b; Ogulei et al. 2006b) as well as indoor particle size distributions (Ogulei et al. 2006a).

The present study obtained information on the sources of particles in the size range 0.012 to 0.470 μm measured at an urban site. This range of particle sizes includes the ultrafine particles (<0.10 μm) that are greater in numbers, but negligible in mass compared to the larger size particles. By investigating this size range of particles, it is possible to more clearly identify and apportion contribution from those sources that contribute more to the particle numbers than to the particle mass concentrations.

DATA DESCRIPTION

The data used for this study were obtained at the New York State Department of Environmental Conservation (NYS DEC) central monitoring site in Rochester, NY (Latitude 43° 08′ 46,″ Longitude 77° 32′ 52″; AIRS ID 270122) between 4th December, 2004 and 30th November, 2005. Figure 1 shows the location of the sampling site as well as the major emission sources. The site was located adjacent to the intersection of the Interstate Highways I-490 and I-590 as well as NY route 96 a major route carrying traffic traveling to and from downtown Rochester. According to 2004 population estimates, the

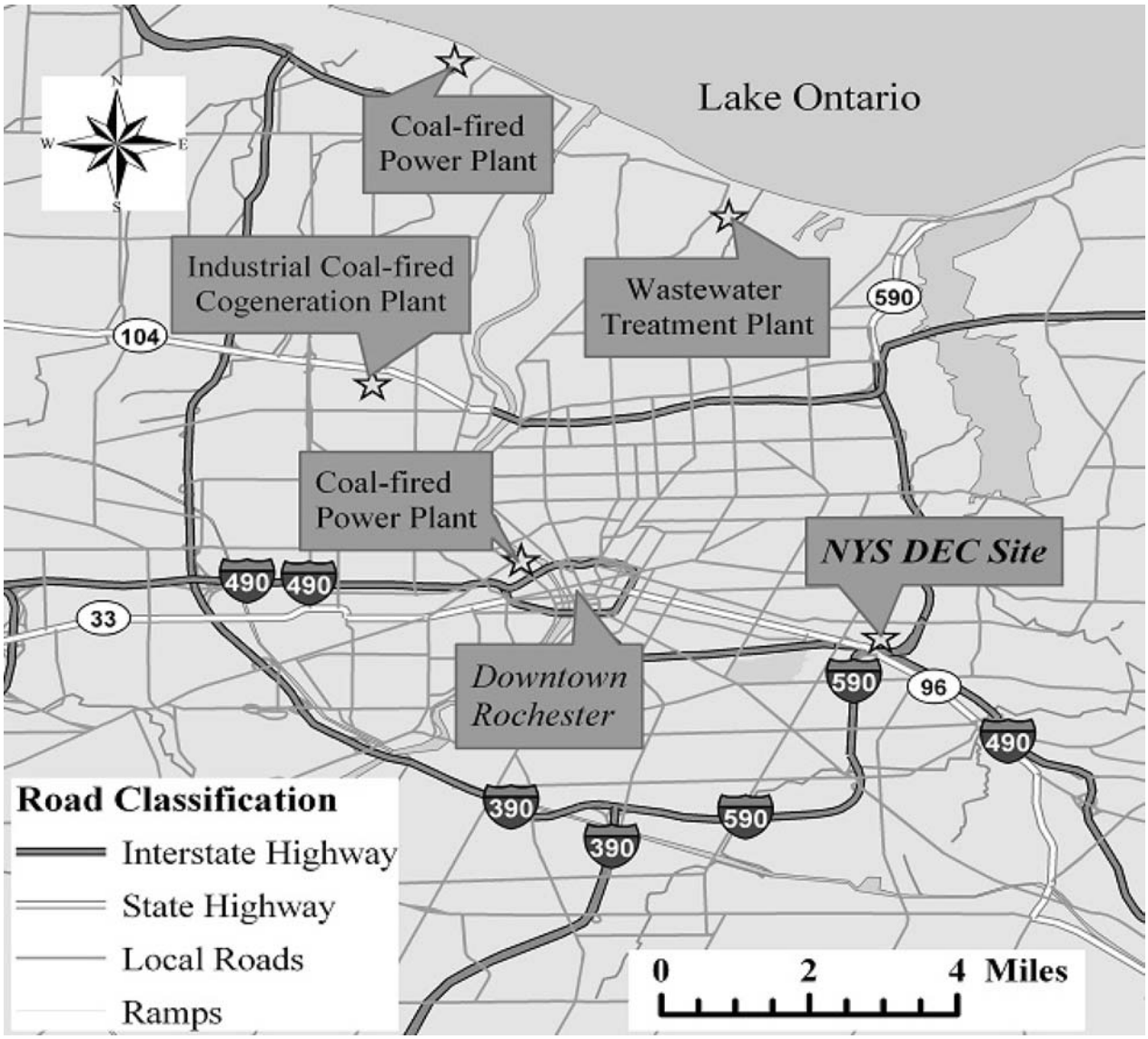

FIG. 1. Map showing the site location and the major emission sources.

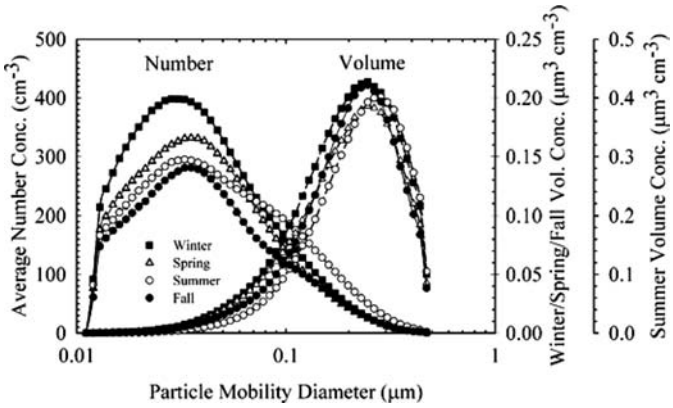

FIG. 2. Plot showing averaged number and volume distributions for the measured 5-minutes data ($d_p = 0.011$–0.47 μm). Typical individual distributions are provided in the supplementary material (Figures S2 to S5).

population of Rochester is about 212,481 (U.S. Census Bureau, http://www.census.gov/), making it the third largest city in New York State.

Size distribution measurements were made every 5 minutes using a scanning mobility particle sizing system (SMPS, TSI Inc.) consisting of an electrostatic classifier (TSI Model 3071), a differential mobility analyzer (DMA) with an impactor orifice size of 0.0457 cm, a ^{85}Kr aerosol neutralizer (TSI Model 3077), and a continuous flow condensation particle counter (CPC; TSI Model 3010). The ambient aerosol was drawn from a 6 m long, 50 mm diameter standard ambient air monitoring sampling manifold. The SMPS was operated at a sheath air to aerosol flow ratio of 10:1 (sheath and sample air flow rates were 5 and 0.5 L min,$^{-1}$ respectively), with the SMPS's inlet located about 2 m from the main inlet. The CPC inlet and sample flow rates were maintained at 1 L min^{-1}. The size range bounds were 10.4 nm (lower) and 0.542 μm (upper) leading to measurement of mid-point particle sizes ranging from 11.1 nm to 0.47 μm (32 channels per decade) at a total scan-up time of 4 minutes per sample. The SMPS system was stationed inside a trailer that was maintained at an average indoor temperature of 23 to 24°C throughout the study period. The calculated particle size distributions were stored and periodically downloaded to Clarkson University via modem.

Generally, the SMPS ran continuously on most days, with an overall data capture rate of 76%. Fifty-three logarithmically-spaced size bins (0.011 to 0.470 μm) were obtained. Figures 2 and 3 summarize the size distribution data used in this study. It can be observed that the mean number concentrations for <0.07 μm particles increased in the winter compared to the spring, summer or fall. This observation is consistent with earlier findings by Jeong et al. (2004, 2006). Overall, the measured concentrations were lowest in the fall. Particles with diameters greater than 0.07 μm were more prevalent during the summer. The highest winter and fall particle concentrations were observed during morning rush hour (8:00 AM). The morning peak shifted to about 7:00 AM and then to 6:00 AM during spring and summer, respectively (Figure 3) probably as a result of earlier sunrise in the spring and summer.

In this study, due to the high fraction of zero concentration values for the 0.011 μm size bin, this size bin was omitted. Thus, the lowest size bin used for the PMF2 model was 0.012 μm.

NYS DEC continuously measured hourly concentrations of gaseous pollutants (CO, O_3, SO_2), meteorological parameters

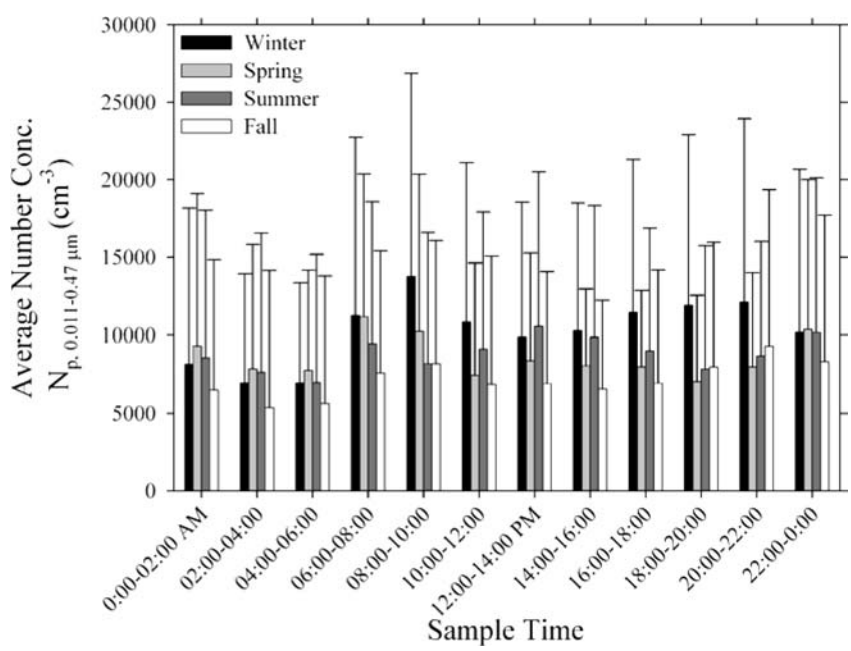

FIG. 3. Bi-hourly average number concentrations for the measured data ($d_p = 0.011$–0.47 μm). The error bars are standard deviations.

(wind speed, wind direction, temperature, and relative humidity), and PM mass at the central site. These hourly data were used to assist in the resolution/identification of the source profiles. The overall wind direction observed during the study period is presented in Figure 4. By obtaining the wind direction corresponding to the highest measured concentrations of these species (upper 25th percentile), the location of the potential sources could be ascertained (Figure 4). Clearly, the sources of each of these species generally seem similar among winter, spring, summer or fall. A significant influence of emissions from the coal-fired power plants, the industrial cogeneration plant, and traffic can be observed.

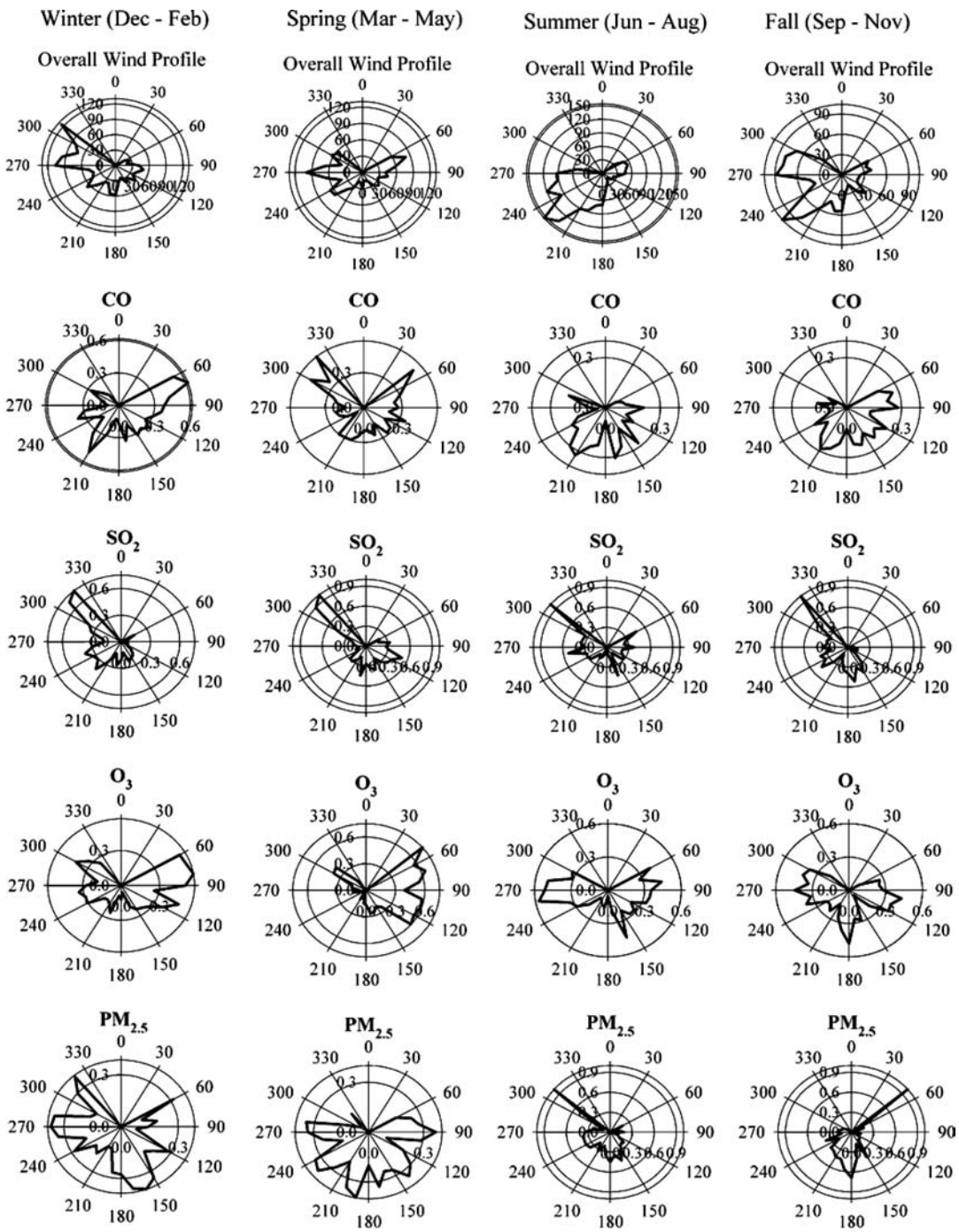

FIG. 4. Directionality of the measured gaseous species, $PM_{2.5}$ mass, and wind profile. The directions were calculated using the Conditional Probability Function (CPF).

The measurement period was divided into four seasons: winter (December, January, February), spring (March, April, May), summer (June, July, August), and fall (September, October, November) so as to avoid experimental uncertainty resulting from too large season-to-season variability in ambient temperature and solar photon intensity that would lead to unstable/nonstationary size distributions. Factor analysis depends on "constant" source profiles characterizing the various sources. It is recognized that some variation in the nature of the source profiles is inevitable. However, large variations such as occur with the significant changes in temperature and photochemical activity that occur over the varying seasons would lead to poorly defined profiles that could be difficult to resolve or multiple profiles that would be impossible to identify with source types. Thus, the four seasons were then analyzed independently for potential sources. For data completeness, only days with at least 95% valid samples were considered (i.e., 71% of days in the winter; 64% in the spring; 83% in the summer; 68% in the fall). Also, in order to be able to utilize the hourly gas speciation and $PM_{2.5}$ mass data, the number concentrations were averaged to one hour resolution. Time averaging in this way was not expected to significantly alter the modal structure of the size distributions of the emission sources. It also eliminated the need to replace any zero number concentration values present in the original 5-minutes data.

MODEL DESCRIPTION

The two-way Positive Matrix Factorization model (PMF2) described by Paatero (1997) was used. The underlying assumption in this approach is that the measured concentrations are linear sums of constant profiles from all of the contributing sources (Hopke, 1985, 1991). This assumption is valid if the size distributions are stationary or quasi-stationary. For p independent sources, PMF2 finds the least squares solution of the component equation:

$$N_{ij} = \sum_{k=1}^{p} g_{ik} f_{kj} + e_{ij} \quad [1]$$

where N_{ij} is the measured submicron particle number concentration of the jth size bin in the ith sample, f_{kj} is the concentration of the jth size bin in material emitted by source k, g_{ik} is the contribution of the kth source to the ith sample and e_{ij} represents the residuals. In order to determine the relationship between the submicron particle number concentrations and the available gaseous pollutant concentration and $PM_{2.5}$ mass data, measured concentrations of CO (ppb), O_3 (ppb), SO_2 (ppb) and $PM_{2.5}$ mass (μg m^{-3}) were included as part of the input matrix. This approach has been described by Zhou et al. (2005b) and Ogulei et al. (2006b).

In this work, all missing concentrations were replaced by interpolated values of the determined concentrations within the same size bin or species. These values were then downweighted by setting their measurement uncertainties as twice the interpolated concentration values. Also, since no measurement uncertainties were available, the required measurement uncertainties were estimated from the equation below (Ogulei et al. 2006a):

$$\sigma_{ij} = \alpha(N_{ij} + \bar{N}_j) \quad [2]$$

where σ is the calculated (estimated) measurement error for size bin j and sample i; $\alpha = 0.01$ (an arbitrary constant explained by Ogulei et al., 2006a); N is the observed number concentration; and $\bar{N}$ is the arithmetic mean of the reported values: N. Equation (2) was also used to estimate measurement errors for the gaseous species ($\alpha = 0.01$) .

The PMF2 algorithm includes several error models that can be used to compute heuristic error estimates (s_{ij}) based on the data points and their original error estimates. The error model equation used in this study was:

$$s_{ij} = \sigma_{ij} + C_3(N_{ij}) \quad [3]$$

where σ_{ij} is the estimated measurement error (Equation [2]), and C_3 is a constant, chosen such that the scaled residuals (e/s) are approximately randomly distributed between -2 and $+2$.

In order to satisfy apportionment conditions (Hopke et al., 1980), the results of PMF2 analysis (source profiles and source contributions) were scaled to the measured concentrations using a scaling constant, s_k, obtained by regressing the measured total number concentrations against the estimated source contributions, g_{ik}, as in Equation (4):

$$N_{ij} = \sum_{k=1}^{p} (S_k) g_{ik} \quad [4]$$

The volume distributions were obtained by assuming spherical particles, such that (Ogulei et al., 2006a):

$$f_{kj,V} = \frac{f_{kj,N}\left(\frac{\pi d_j^3}{6}\right)}{\sum_{j=1}^{m} f_{kj,N}\left(\frac{\pi d_j^3}{6}\right)} = \frac{f_{kj,N} d_j^3}{\sum_{j=1}^{m}\left(f_{kj,N} d_j^3\right)} \quad [5]$$

where $f_{kj,V}$ and $f_{kj,N}$ are, respectively, the volume and number fractions of size bin j in source k; d_j is the measured particle diameter.

Solving for the Optimum Number of Factors

The four data sets (winter, spring, summer, fall) were independently analyzed in the robust mode (Huber 1981; Paatero 1997). A thorough description of the method used to estimate the optimum number of factors, p, has been provided by Ogulei et al. (2006a). Expected (theoretical) values of the residual sum of squares, Q, were 83328 (winter), 79296 (spring), 102144 (summer), and 67364 (fall). For each value of p, different values of C_3 (Equation [3]) from 0.01 to 0.5 were tested while

comparing the obtained Q-value to the theoretical value. Final C_3 values were 0.1 (winter), 0.105 (spring), 0.191 (summer), and 0.1 (fall) for $p = 7$ in the winter, spring and summer, and $p = 9$ in the fall. Rotations were imposed to the emerging solutions by adjusting the FPEAK value (Paatero et al. 2002) so as to obtain more physically realistic and independent solutions. Final FPEAK values were 0.1, 0.1, 0.0, and 0.0 with corresponding Q-values of 82610, 79321, 102758, and 68000 for winter, spring, summer and fall, respectively.

Estimating Potential Source Locations

The Conditional Probability Function (CPF; Ashbaugh et al. 1985) was used to estimate the wind direction that produced the maxima in the observed number concentrations. These directions were then taken as the most probable locations of the emission sources. In general, CPF is used to estimate the probability that a given source contribution from a given wind direction will exceed a predetermined threshold criterion. The defining equation is:

$$\mathrm{CPF}_{\Delta\theta} = \frac{m_{\Delta\theta}}{n_{\Delta\theta}} \qquad [6]$$

where $m_{\Delta\theta}$ is the number of occurrences from wind sector $\Delta\theta$ that exceeded a defined threshold criterion (upper 25th percentile for this study), and $n_{\Delta\theta}$ is the total number of data points from the same wind sector. The CPF value was set to zero if $n_{\Delta\theta}$ was less than 10. Thirty-six equal wind sectors were used, starting at 0°. Wind speeds less than 1.0 m/s were excluded to minimize stagnation effects at lower wind speeds. CPF analyses were performed on the "raw" gaseous and $PM_{2.5}$ mass concentrations (Figure 4) and the resolved source contributions (i.e., g_{ik}-values).

RESULTS AND DISCUSSION

By independently investigating the four seasonal data sets, a total of ten different sources were identified. These source types included two traffic factors, two nucleation factors, industrial emissions, residential/commercial heating, secondary nitrate, secondary sulfate, ozone-rich secondary aerosol, and regionally transported aerosol. A summary of the pertinent information used for source identification is provided in Table 1. In general, the source types were identified through information derived from (1) modal characteristics of the observed size distributions, (2) Pearson pair-wise product moment correlation between each source factor and the measured gaseous species and $PM_{2.5}$ mass concentrations, (3) the diurnal behavior of the source, (4) source directionality as provided by the CPF, and (5) source contribution to the total apportioned particle concentrations. The sources resolved in this study were generally characterized by similar number modes for either winter, spring, summer, or fall. A summary of the average number contributions from all of these sources is presented in Table 2.

The size distribution for nucleation was dominated by particles close to 10 nm in diameter (Figure 5). As time progressed during the day, these particles gradually grew to larger sizes resulting in volume modes in the accumulation mode range (see Supplementary Figures S6 and S7). In general, a nucleation factor features only the smallest particles (Zhou et al. 2005a, 2005b; Ogulei et al. 2006b). Nucleation was frequently observed during the study period. Morning nucleation episodes were generally observed during the winter while afternoon episodes were prevalent during the spring, summer and fall (see Supplementary Figures S2 to S5). The two nucleation factors could easily be distinguished from their diurnal patterns (Figure 6). The first nucleation factor (nucleation 1) correlates well with morning traffic rush hour for Rochester suggesting that cooling of tail-pipe emissions may have induced nucleation activity in the vicinity of the highways (Figure 1). Similar observations have previously been reported by Jeong et al. (2004, 2006) in which morning nucleation events in Rochester were found to produce particles in the size range 11 to 30 nm. The CPF plots for the nucleation factors point to the intersection of the interstate highways I-490 and I-590 as well as NY route 96 (Figures 1, 7, and 8). The rate of formation of such particles is dependent on both the type of the vehicle and the prevailing meteorological conditions (Shi and Harrison 1999; Charron and Harrison 2003).

The second nucleation factor (nucleation 2) shows mid-afternoon high values (Figure 6) that are typical of processes that are driven by daytime photochemistry coupled with a steady wind direction. This factor was only resolved for the summer and fall periods. It was not possible to separate the first nucleation factor into two factors in winter and spring. Thus, the first nucleation factor probably represents both morning and afternoon nucleation, while the second factor clearly refers to afternoon nucleation. This factor was highly correlated with SO_2, with the highest Pearson correlation coefficient of 0.97 recorded in the fall (Table 1).

Two traffic factors were resolved. Traffic 1 shows major number modes at about 28 nm (winter), 26 nm (spring), 25 nm (summer) and 26 nm (fall), and the minor mode at about 0.1 μm (Figure 5). The volume distributions are at-least tri-modal for this factor. In contrast, traffic 2 is characterized by major number modes at about 84 nm (winter), 67 nm (spring), 78 nm (summer), and 58 nm (fall). The minor modes are, respectively, 21, 21, 16, and 20 nm. Volume distributions for this factor were approximately bimodal. The modal nature of these two profiles suggests that the two traffic factors may be distinguished as local (traffic 1) and distant (traffic 2) sources. The source profiles are generally dominated by CO and $PM_{2.5}$ mass emissions, especially during the winter (Table 1 and Figure 9) when very low ambient temperatures lead to incomplete fuel combustion. The high amount of SO_2 in traffic 1 may suggest that this factor could also be related to diesel emissions. Most particles from diesel engines are in the size range ~20–130 nm (Morawska et al. 1998), while most particles from gasoline engines are in the size

TABLE 1

Summary of the information used for source identification. Bold-faced percentages are the percentage contribution of each factor to the total apportioned number concentrations

Source ID	Major number modes (μm)	Highest two positive Pearson coefficients				Diurnal Profile	Dominant Directions
		Winter	Spring	Summer	Fall		
Nucleation 1	0.01–0.02 (tri-modal)	CO (0.37) $PM_{2.5}$ (0.26) **21.0%**	CO (0.32) SO_2 (0.24) **18.4%**	CO (0.25) SO_2 (0.22) **15.7%**	CO (0.44) SO_2 (0.18) **15.0%**	Morning, afternoon peaks	South, Southwest
Nucleation 2*	Multiple modes	— **0.0%**	— **0.0%**	SO_2 (0.36)* CO (0.08)* **22.0%***	SO_2 (0.97) $PM_{2.5}$ (0.22) **0.4%**	Midafternoon high	Northwest
Traffic 1*	0.02–0.03 (bimodal)	CO (0.45) $PM_{2.5}$ (0.38) **31.1%**	CO (0.26) SO_2 (0.20) **24.8%**	SO_2 (0.36)* CO (0.08)* **22.0%***	CO (0.32) SO_2 (0.22) **24.2%**	Pronounced morning peak	Northwest, South
Traffic 2	0.05–0.08 (bimodal)	CO (0.65) $PM_{2.5}$ (0.63) **16.4%**	$PM_{2.5}$ (0.47) CO (0.29) **19.2%**	CO (0.26) SO_2 (0.09) **23.3%**	CO (0.55) $PM_{2.5}$ (0.26) **16.8%**	Daytime low, evening/night time high	East, Southwest
Industrial Emissions	0.04–0.05 (~2–3 modes)	CO (0.40) $PM_{2.5}$ (0.38) **24.5%**	CO (0.38) $PM_{2.5}$ (0.24) **25.3%**	SO_2 (0.24) CO (0.19) **21.4%**	CO (0.39) $PM_{2.5}$ (0.19) **24.6%**	Undefined/ Inconsistent	Northwest
Residential and/or Commercial Heating	0.1–0.2 (tri-modal)	$PM_{2.5}$ (0.72) CO (0.39) **5.3%**	$PM_{2.5}$ (0.69) CO (0.48) **9.2%**	— **0.0%**	CO (0.60) $PM_{2.5}$ (0.60) **12.2%**	Evening/night time High	East, West, South
Secondary Nitrate	0.2–0.3 (~4 modes)	$PM_{2.5}$ (0.76) CO (0.46) **0.8%**	$PM_{2.5}$ (0.73) CO (0.31) **1.7%**	— **0.0%**	$PM_{2.5}$ (0.77) CO (0.59) **1.1%**	Daytime low, Nighttime high	South, Southeast, Northeast
O_3-rich Secondary Aerosol	Multiple modes	O_3 (0.91) **0.8%**	O_3 (0.70) SO_2 (0.08) **1.4%**	O_3 (0.82) $PM_{2.5}$ (0.47) **4.7%**	O_3 (0.92) $PM_{2.5}$ (0.15) **1.0%**	Daytime high, Summer high	Northwest, Northeast
Secondary Sulfate	0.1–0.2 (~3 modes)	— **0.0%**	— **0.0%**	$PM_{2.5}$ (0.51) O_3 (0.36) **10.9%**	$PM_{2.5}$ (0.85) CO (0.52) **4.7%**	Weak	Southwest, South, Northeast
Regional Transport	0.2–0.3 (~2–3 modes)	— **0.0%**	— **0.0%**	$PM_{2.5}$ (0.75) O_3 (0.29) **1.9%**	— **0.0%**	Weak	Southwest

*For summer, these sources were resolved as one factor.

TABLE 2
Average source contributions (cm^{-3}) from all the resolved sources. Numbers in parentheses are standard errors

Resolved source	Winter (Dec.–Feb.)	Spring (Mar.–May)	Summer (Jun–Aug.)	Fall (Sep.–Nov.)
N[1]	1488	1416	1824	1444
Nucleation 1	2162 (59.5)	1588 (46.6)	1365 (37.5)	1087 (30.8)
Nucleation 2*	N/A[2]	N/A	1908 (43.4)*	32.4 (0.8)
Traffic 1*	3206 (84.6)	2145 (54.6)	1908 (43.4)*	1748 (48.6)
Traffic 2	1689 (53.4)	1657 (39.1)	2027 (85.8)	1211 (35.4)
Industrial Emissions	2526 (66.8)	2183 (55.0)	1861 (58.9)	1779 (56.1)
Residential and/or Commercial Heating	550 (12.0)	797 (19.9)	N/A	880 (23.4)
Secondary Nitrate	87.1 (2.4)	149.7 (3.5)	N/A	77.1 (1.9)
O_3-rich Secondary Aerosol	82.1 (1.3)	123.2 (2.0)	409.2 (6.0)	73.3 (1.4)
Secondary Sulfate	N/A	N/A	951 (18.8)	337 (10.2)
Regional Transport	N/A	N/A	166.2 (3.5)	N/A

[1]Indicates total number of samples.
[2]Indicates that factor was not resolved for the respective data set.
*For summer, *Nucleation 2* and *Traffic 1* were resolved as one factor.

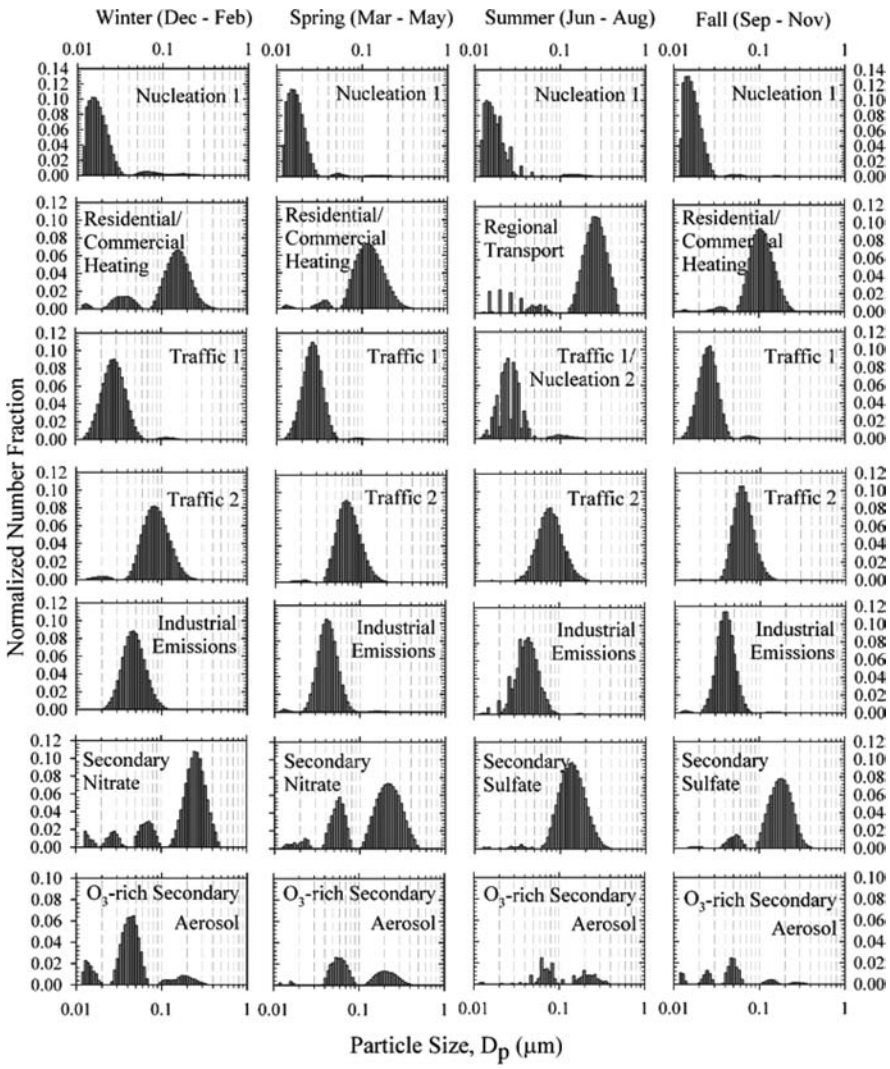

FIG. 5. Particle number profiles of all the resolved sources.

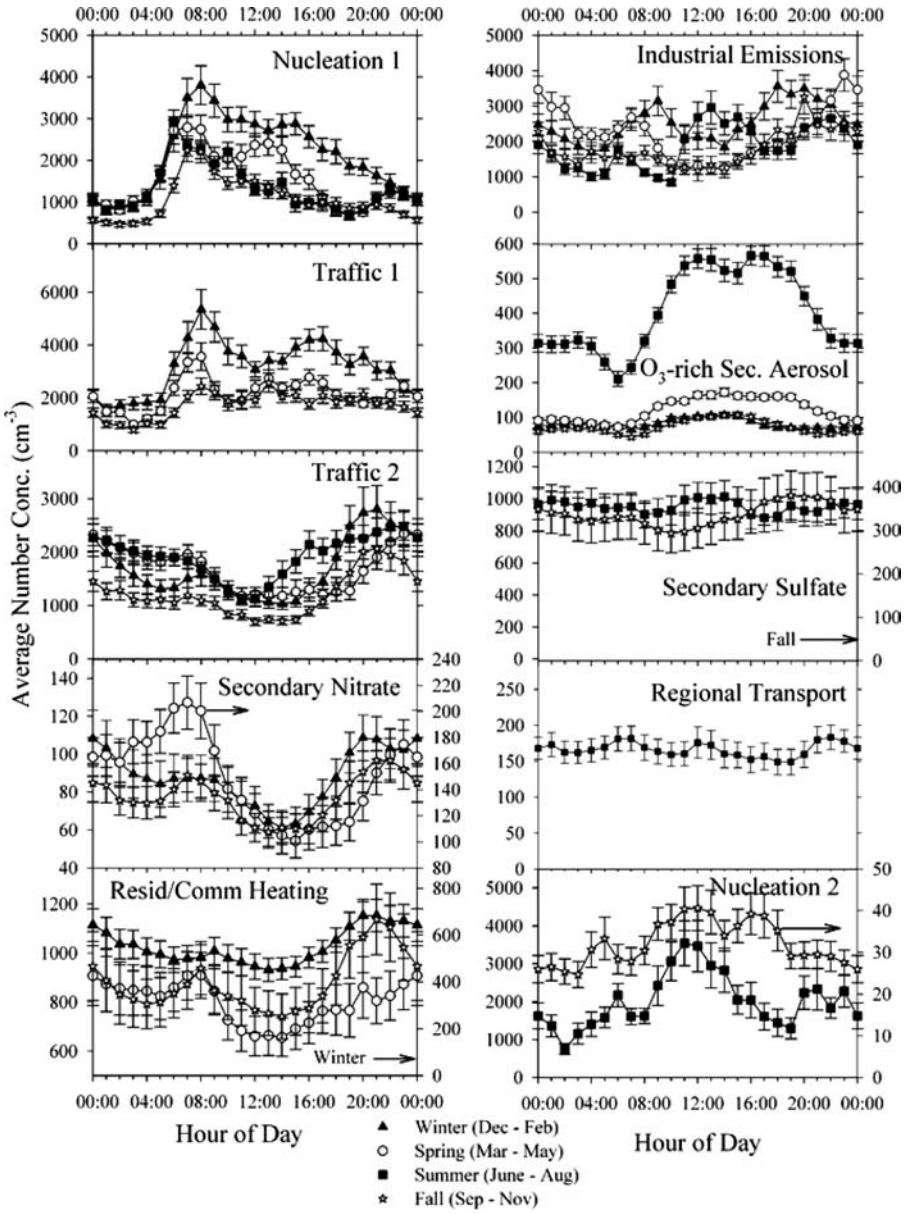

FIG. 6. Diurnal behavior of the resolved g_{ik} factors.

range ~20–60 nm (Ristovski et al. 1998). The two traffic factors can also be distinguished by observing the corresponding CPF plots (Figure 8). The directionality of traffic 1 corresponds to the location of downtown Rochester as well as the direction of NY route 96, which carries traffic traveling to and from the downtown area. Thus, this factor may also represent local traffic. The directionality of traffic 2, however, corresponds to the location of the Interstate Highways I-490 and I-590 suggesting that this factor may also represent emissions from local highway traffic. The nighttime high contributions (Figure 6) to this factor (traffic 2) are attributable, in part, to nocturnal commercial truck traffic that traverses the interstate highways around Rochester. Average weekday contributions from traffic 1 exceeded weekend values by factors of 1.4, 1.6, 1.1, and 1.1 in winter, spring, summer and fall, respectively, while there were no significant weekday-weekend differences observed for traffic 2 (Figure 10). The total contribution of traffic to the observed particle number concentrations was 47.5% in winter, 44.0% in spring, 45.3% in summer, and 41.0% in the fall (Table 1). Although the mode of the summer-resolved traffic 1 factor was similar to the other traffic 1 factors, its diurnal profile was similar to that of the nucleation 2 factor, with a mid-day maximum and a relatively significant correlation with SO_2. Thus, it is suggested that traffic 1 and nucleation 2 are mixed in one factor during the summer. The results presented here are generally in agreement with reported size distributions downwind of traffic highways

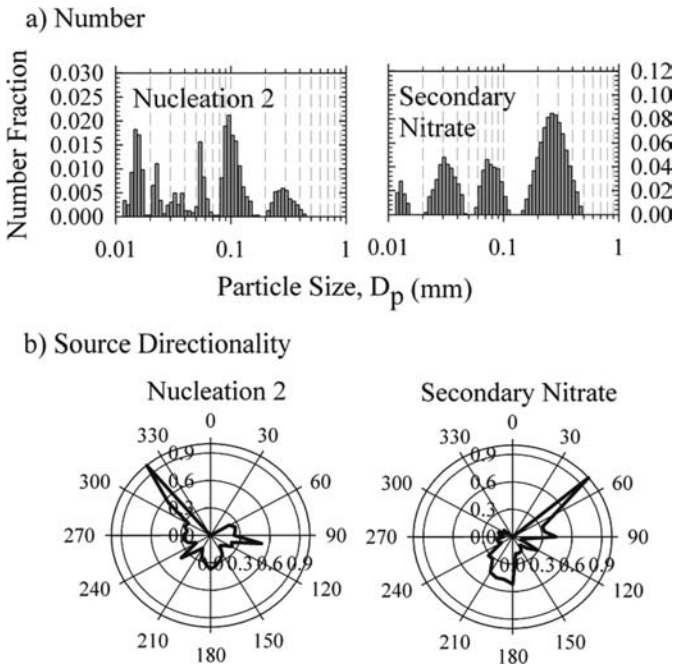

FIG. 7. Profiles for the *nucleation 2* and *secondary nitrate* factors resolved during the fall season.

(Janhäll et al. 2004; Zhang et al. 2004; Rosenbohm et al. 2005).

The major number modes for industrial emissions were 47 nm (winter), 41 nm (spring), 44 nm (summer), and 41 nm (fall). The volume distributions were approximately bimodal with volume modes at about 0.06 and 0.2 μm (winter), 0.05 and 0.2 μm (spring), 0.05 and 0.25 μm (summer), and 0.05 and 0.14 μm (fall). Industrial emissions were clearly dominated by emissions from coal-fired power plants and a coal-fired cogeneration plant that were located to the northwest of the sampling site (Figures 1 and 11). According to the United States Environmental Protection Agency (EPA), these two facilities represent the largest point emission sources of fine (<2.5 μm) particles in Rochester (http://www.epa.gov/air/data/).

The species profiles for this factor show high fractions of CO, SO_2 and $PM_{2.5}$ for the entire period investigated (Figure 9). The EPA's 1999 emissions estimates show that coal combustion in the Rochester area accounts for about 81.4% of all point source $PM_{2.5}$ emissions, and 15.7% of the overall PM emissions. Coal combustion also accounts for 98.6% of point source SO_2 emissions, and 86.1% of the region's overall annual SO_2 burden. The potential source locations indicated by the CPF plots (Figure 11) is consistent with that of SO_2 (Figure 4). No significant weekday-weekend differences were observed, although source contributions tended to decrease from the winter to the spring to the summer (Figure 10) probably due to the gradual increase in average mixing depth.

Recent industrial stack measurements have found stack emissions from oil combustion facilities equipped with standard control devices (e.g., scrubbers) to mainly consist of particles less than 0.2 μm in diameter, and comprising of bimodal size distributions with count median modes at about 20–30 and 50 nm (Morawska et al. 2006). The downwind distributions (4.5 Km from the oil combustion facility studied) were also bimodal with count median modes approximately equivalent to the stack values. Other industrial emissions studies, however, show that the size distribution of particles emitted from industrial facilities is dependent on the flue gas temperature, combustor configuration and the process control settings (Miller et al. 1998; Linak et al. 2000; Maguhn et al. 2003). Thus, the season-to-season similarity of the size distributions obtained in this study suggests that these emissions are dominated by a single group of sources, as illustrated by the CPF plots (Figure 11).

The factor representing residential and/or commercial heating was only resolved during the winter (December to February), spring (March to May) and fall (September to November). This factor was characterized by an approximately tri-modal number profile, but a unimodal volume distribution. The species profile for this factor shows a high loading of SO_2 and $PM_{2.5}$ (Figure 9). Most residences and commercial buildings in Rochester are heated through wood, natural gas, and oil combustion. Residential wood combustion is a major source of $PM_{2.5}$ mass in the region contributing 23.1% of the overall annual $PM_{2.5}$ burden while oil combustion accounts for 10.2% of the overall SO_2 burden in the Rochester area (http://www.epa.gov/air/data/). The diurnal profile shows minimum contributions during the day (Figure 6) that would be expected from urban residential contributions. Also, relatively higher concentrations are obtained on weekends (Figure 10). Kleeman et al. (1999) report number modes between 0.1–1 μm from wood combustion. The directionality of this factor (Figure 8) further permits distinction between this factor and combustion sources included under the industrial emissions factor.

The secondary nitrate factor was associated with a volume mode in the accumulation range (0.3 μm). The number profiles, however, show presence of both Aitken and accumulation mode particles (Figures 5 and 7). This observation suggests that both local and distant/regional particles may be present in this factor. This factor is thought to represent secondary nitrate in, which the Aitken mode particles may have been formed from atmospheric processing of local NOx emissions. Particles in the accumulation range are capable of being airborne for longer periods of time and can be transported for long distances. The directions shown by the CPF plots for this factor (Figures 7 and 11) coincide with the directions of major highways (winter, spring, fall) as well as industrial and major cities that are to the south-east of the site (winter, spring). Thus, this nitrate can also be thought of as having been formed during the transport of its precursor gases, NH_3 and NOx from distant sources.

The averaged source contribution consists of a high contribution in the early morning hours (Figure 6) when a combination of low ambient temperature and high relative humidity favors

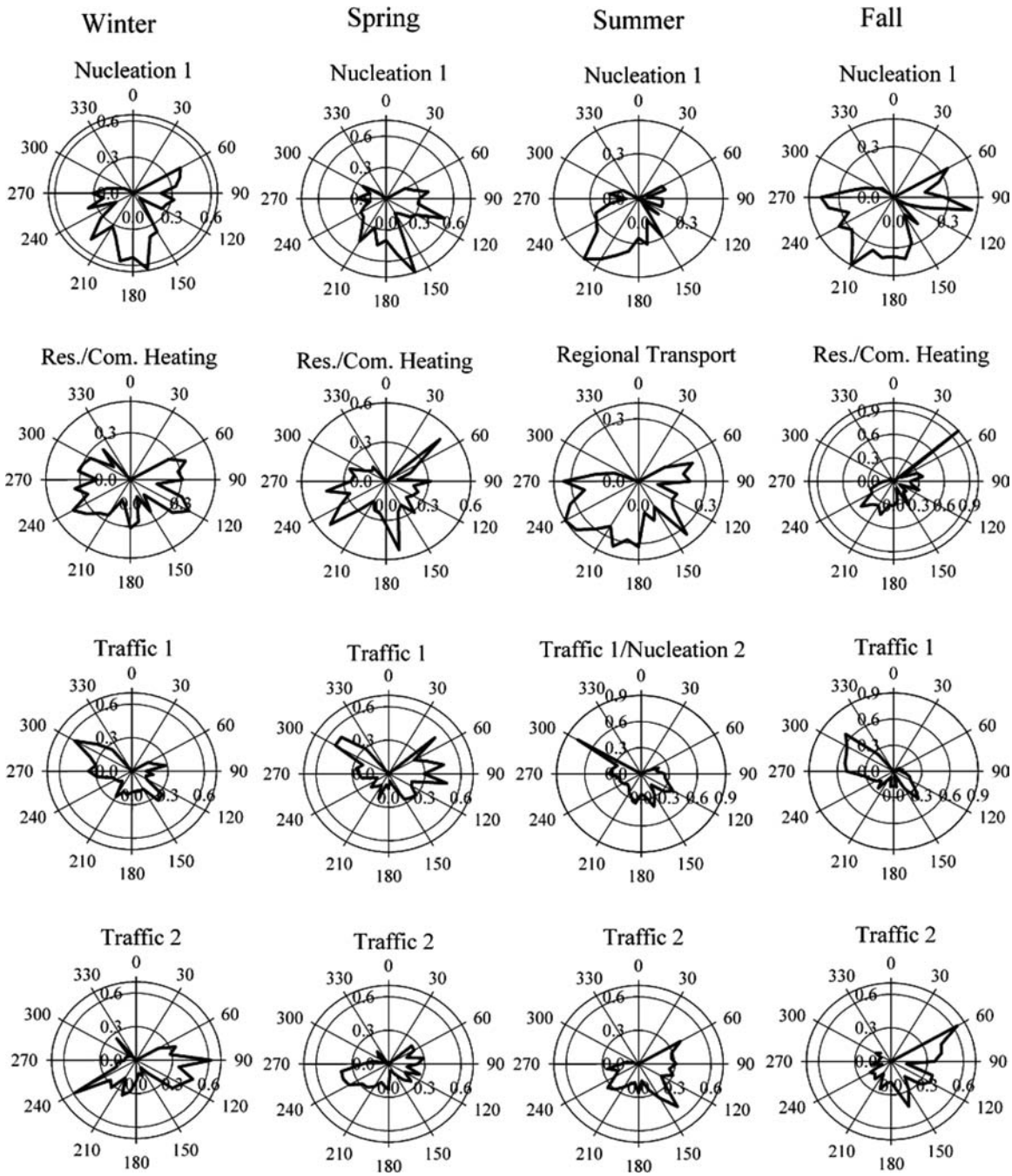

FIG. 8. Directionality of the resolved factors.

the formation of particulate nitrate (Moya et al. 2001; Tolocka et al. 2004; Wittig et al. 2004; Zhou et al. 2005b). The morning peak has also been attributed to the morning NOx pulse from rush hour traffic (Rattigan et al. 2006). Minimum concentrations were observed during the day when higher temperatures and lower relative humidity may have led to the dissociation of particulate ammonium nitrate back to ammonia and nitric acid. This factor represents about 0.8% of the apportioned number concentrations during the winter period, 1.7% during the spring, and about 1.1% of the apportioned number concentrations during the fall period (Table 1).

The spring contribution was much higher than the winter or fall contribution, with the highest contribution registered in March (~200 particles per cm^3). One possible explanation for the existence of the spring maximum is illustrated by Figure 12 in which the average relative humidity (RH) and the deliquescence

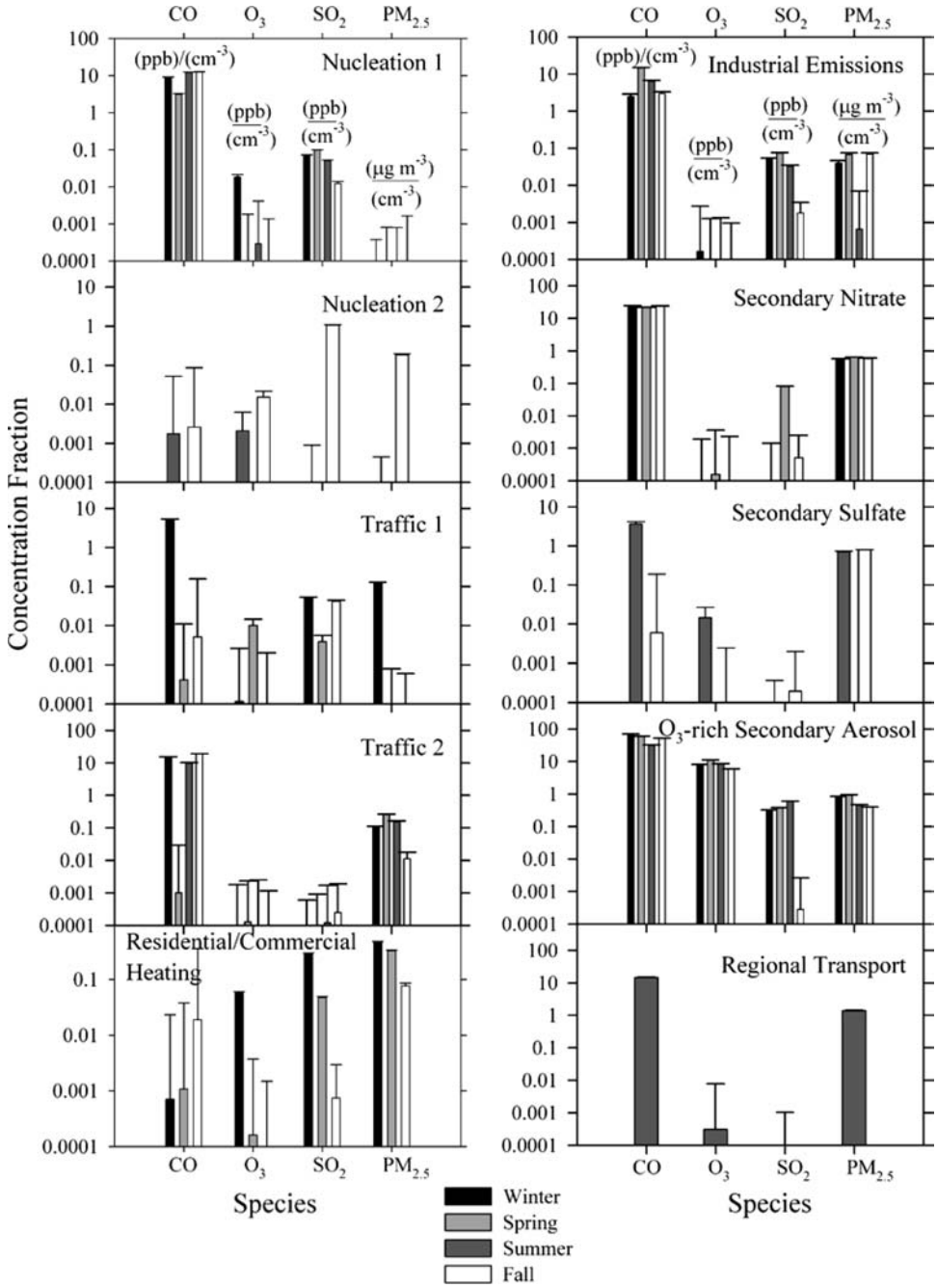

FIG. 9. Profiles of the measured gaseous species and $PM_{2.5}$ mass as resolved using PMF2.

relative humidity ($RH^{(D)}$) are plotted for each month considered in this study. $RH^{(D)}$ values are calculated from the equation (Seinfeld and Pandis, 1998):

$$RH^{(D)} = \exp\left\{\frac{723.7}{T(K)} + 1.6954\right\} \quad [7]$$

where T is the ambient temperature (Kelvin). δ^*_{RH} is then obtained by subtracting RH from the corresponding value of $RH^{(D)}$.

The equilibrium state of pure ammonium nitrate is a solid if RH is less than $RH^{(D)}$ (Stelson and Seinfeld, 1982; Tang and Munkelwitz, 1993; Seinfeld and Pandis, 1998; Ansari and Pandis 2000). Thus, a plot of the difference between $RH^{(D)}$ and RH (or δ^*_{RH}), as shown in Figure 12 (circles), provides a good estimate of the ammonium nitrate trend. In the present case, a spring maximum would be expected from the $PM_{0.5}$ nitrate studied whereas virtually no $PM_{0.5}$ nitrate exists in particulate form during the summer (Figure 12). The predicted $PM_{0.5}$ nitrate contribution is

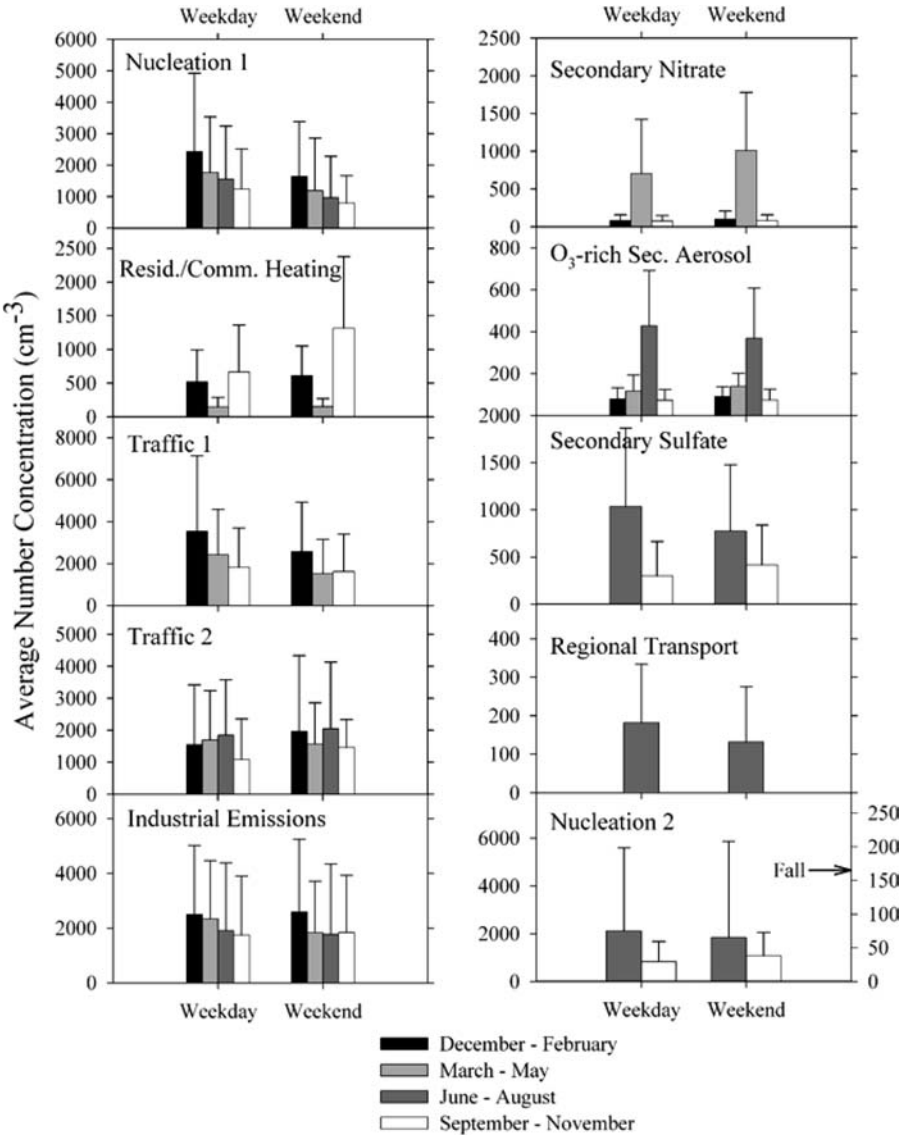

FIG. 10. Average weekday and weekend contributions for all the factors.

seen to drop when the ambient temperature rises above 14°C, with the minimum contribution recorded at 23–25°C. It can be observed (Figure 12) that there is a drop in ambient temperature from February to March, although photointensity would be expected to be higher in March than in February or January, that could lead to more HNO_3 production in March. A large number of missing values in the available $PM_{2.5}$ nitrate data prevented direct comparison between the nitrate concentrations predicted in this study (Figure 12) and the measured $PM_{2.5}$ nitrate mass concentrations.

It should be noted that the above discussion represents only a possible explanation for the seasonal behavior of the $PM_{0.5}$ nitrate predicted in this study, and should not be considered conclusive. Further study is necessary to explore the effect of other drivers to nitrate concentrations, namely; total available nitrate, etc. Although the predicted seasonal trend in the Rochester $PM_{0.5}$ nitrate is comparable to the seasonal pattern reported by Rattigan et al. (2006) for $PM_{2.5}$ nitrate mass concentrations in New York State, most studies conducted in the eastern United States have reported a winter maximum in the observed $PM_{2.5}$ nitrate concentrations (e.g., Tolocka et al. 2004; Wittig et al. 2004). Thus, future study may be necessary to further investigate the seasonality of the secondary nitrate predicted in the present analysis.

The secondary sulfate factor was only resolved for the summer and fall aerosol and was characterized by major number modes at about 0.14 and 0.18 μm in summer and fall, respectively. The volume distribution was largely unimodal with a mode close to 0.2 μm. These sulfate particles may have been formed through atmospheric processing of local or distant SO_2

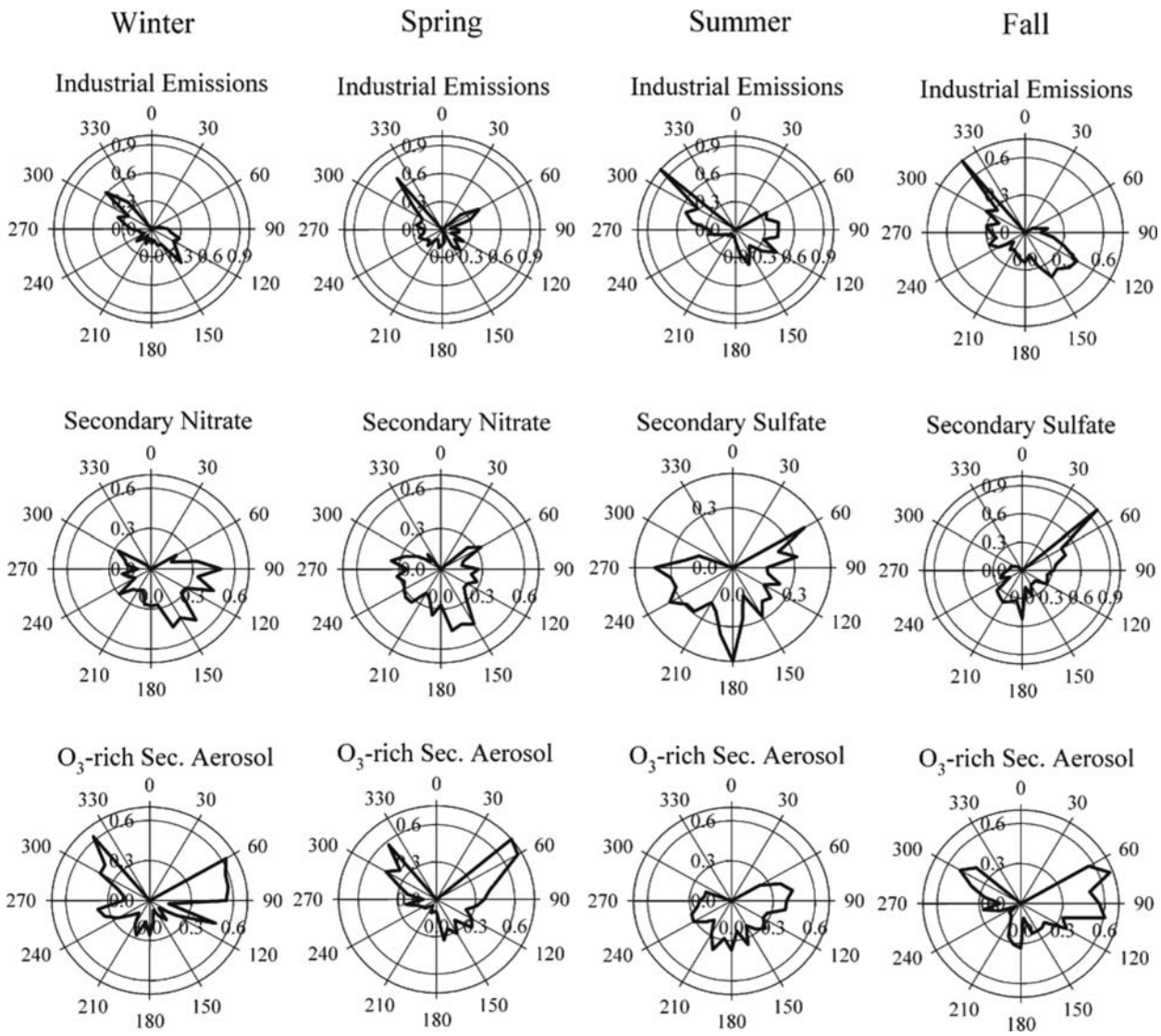

FIG. 11. Directionality of the resolved factors.

emissions (Zhuang et al. 1999; Kerminen et al. 2000). Local sulfate emissions result when SO_2 adsorbs to newly formed combustion particles and undergo oxidation into sulfate (Kerminen et al. 2000). This might perhaps explain the directionality of the CPF plot for this factor (Figure 11) since the directions shown correspond to the locations of local sources of combustion-derived particles (chiefly from traffic). The presence of an accumulation mode implies that these particles have grown to larger sizes through coagulation and other processes. The diurnal profile (Figure 6) shows an apparent day-time summer maximum for this factor, which suggests downward mixing as the boundary layer increases. This factor accounts for about 11% of the apportioned aerosol particles during the summer and 5% in the fall.

Regionally transported material was mostly characterized by accumulation mode particles, with the major number mode close to 0.2 μm. Because these particles are too small for inertial deposition and too big for diffusive removal processes, they are capable of remaining airborne for longer periods of time. No clear diurnal profile is observed (Figure 6). Air parcel backtrajectories, calculated using the NOAA HYSPLIT model (Draxler and Rolph, 2003) for the periods of high source contributions, showed transport of air masses from the industrial midwest (Figure 13). It is possible that these particles may be loaded with sulfate resulting from atmospheric processing of SO_2 emitted by the major coal-fired power plants located in the industrial midwest. This factor was highly correlated with $PM_{2.5}$ mass, with an r^2-value of 0.75.

Finally, a factor that was highly enriched with O_3 was resolved from each of the data sets used in this study. This factor could not be attributed to any specific source and thus, was subjectively called "Ozone-rich secondary aerosol." Very good

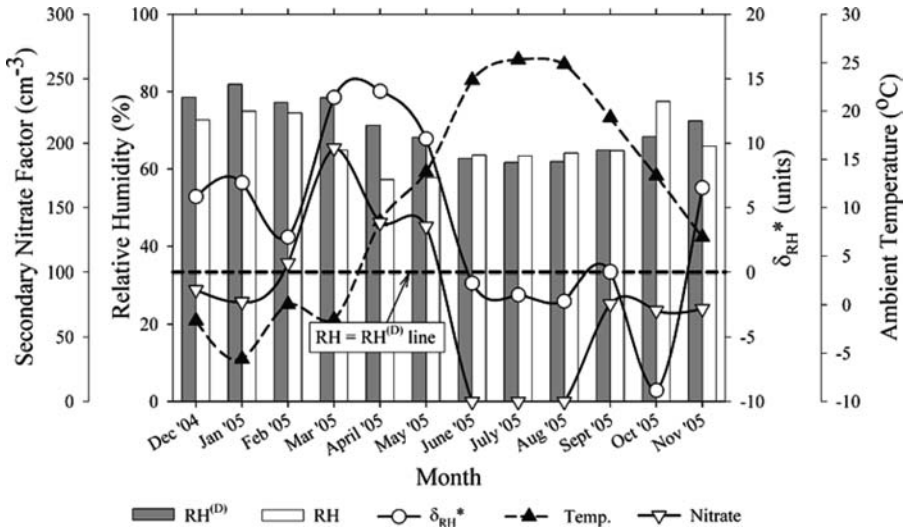

FIG. 12. Plot showing averaged monthly relative humidity (RH) and the deliquescence relative humidity ($RH^{(D)}$) over the study period. The predicted secondary nitrate contribution tracks fairly well with δRH.

associations were observed between this factor and O_3, with Pearson product moment correlation coefficients being 0.91 (winter), 0.70 (spring), 0.82 (summer), and 0.92 (fall). Resolved concentrations increased from the winter to the spring to the summer with day-time maximums (Table 2 and Figure 6). This observation underscores the important role of photochemistry in ozone formation. This ozone may have been formed from photochemically catalyzed oxidation of anthropogenic volatile organic compounds (VOCs from vehicle exhaust, evaporation of solvents and gasoline, etc.) by the OH radical in NOx-rich environments. Fall values were comparable to winter values, and no significant weekday-weekend differences were observed (Figure 10) suggesting that this factor may represent an ozone background.

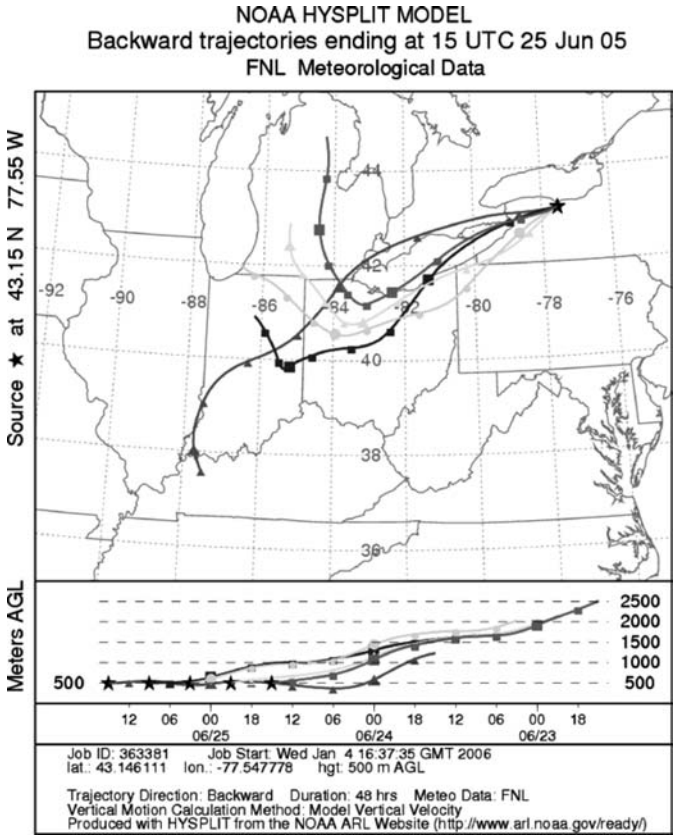

FIG. 13. Typical NOAA HYSPLIT back-trajectories showing particle transport from the industrial midwest. Plot shows five trajectories started every 6 hours.

CONCLUSION

An advanced bilinear receptor model has been used to apportion submicron (0.01–0.5 μm) particle number concentrations measured in Rochester, NY. The present study has successfully identified the major sources of these particles contributing to the measured particle number concentrations. The majority of the resolved sources were found to be attributable to local sources. The results from this study show little season-to-season variability in the number modes of particles emitted from any given source.

The major particle sources include traffic, nucleation, industrial emissions, residential/commercial heating, secondary nitrate, secondary sulfate, ozone-rich secondary aerosol, and regionally transported aerosol. The most important sources were found to be nucleation, traffic and industrial emissions cumulatively accounting for as much as 93.0%, 87.6%, 82.4%, and 81.0% of the apportioned concentrations during the winter, spring, summer, and fall, respectively.

Nucleation episodes led to most of the particles close to 10 nm in diameter, while traffic was mainly responsible for particles in the size range 20 to 40 nm. Although the diurnal pattern of each of the two traffic factors closely followed traffic rush

hour for Rochester, their modes were different suggesting that these factors might represent local and remote emissions. Further studies may be necessary to determine if these factors may also represent diesel and gasoline vehicle emissions.

Industrial emissions were largely attributable to the local SO_2 and CO point sources in Rochester, namely coal-fired power plants and a cogeneration power plant. The highest average concentrations from these emissions were greater in the winter and spring than in the summer and fall, probably (in part) due to lower winter mixing height. The average concentrations were insignificantly different between weekday and weekend.

REFERENCES

Ansari, A. S., and Pandis, S. N. (2000). The effect of Metastable Equilibrium States on the Partitioning of Nitrate between the Gas and Aerosol Phases, *Atmos. Environ.* 34:157–168.

Ashbaugh, L. L., Malm, W. C., and Sadeh, W. Z. (1985). A Residence Time Probability Analysis of Sulfur Concentrations at Grand Canyon National Park, *Atmos. Environ.* 19:1263–1270.

Charron, A., and Harrison, R. M. (2003). Primary Particle Formation from Vehicle Emissions During Exhaust Dilution in the Roadside Atmosphere, *Atmos. Environ.* 37:4109–4119.

Draxler, R. R., and Rolph, G. D. (2003). HYSPLIT (HYbrid Single-Particle Lagrangian Integrated Trajectory) Model access via NOAA ARL READY Website (http://www.arl.noaa.gov/ready/hysplit4.html). NOAA Air Resources Laboratory, Silver Spring, MD.

Hien, P. D., Bac, V. T., and Thinh, N. T. H. (2004). PMF Receptor Modelling of Fine and Coarse PM in Air Masses Governing Monsoon Conditions in Hanoi, Northern Vietnam, *Atmos. Environ.* 38:189–201.

Hien, P. D., Bac, V. T., and. Thinh, N. T. H. (2005). Investigation of Sulfate and Nitrate Formation on Mineral Dust Particles by Receptor Modeling, *Atmos. Environ.* 39:7231–7239.

Hopke, P. K., Lamb, R. E., and Natusch, D. F. C. (1980). Multi Elemental Characterization of Urban Roadway Dust, *Environ. Sci. Technol.* 14:164–172.

Hopke, P. K. (1985). *Receptor Modeling in Environmental Chemistry*. John Wiley & Sons, New York.

Hopke, P. K., ed. (1991). *Receptor Modeling for Air Quality Management*. Elsevier Science, Amsterdam.

Huber, P. J. (1981). *Robust Statistics*. John Wiley and Sons, New York.

Ibald-Mulli, A., Wichmann, H. E., Kreyling, W., and Peters, A. (2002). Epidemiological Evidence on Health Effects of Ultrafine Particles, *J. Aerosol Med.* 15:189–201.

Janhäll, S., Jonsson, Å. M., Molnàr, P., Svensson, E. A., and Hallquist, M. (2004). Size Resolved Traffic Emission Factors of Submicrometer Particles, *Atmos. Environ.* 38:4331–4340.

Jeong, C.-H., Hopke, P. K., Chalupa, D., and Utell, M. (2004). Characteristics of Nucleation and Growth Events of Ultrafine Particles in Rochester, NY, *Environ. Sci. Technol.* 38:1933–1940.

Jeong, C.-H., Evans, G. J., Hopke, P. K., Chalupa, D., and Utell, M. (2006). Influence of Atmospheric Dispersion and New Particle Formation Events on Ambient Particle Number Concentration in Rochester, USA and Toronto, Canada, *J. Air and Waste Manage. Assoc.* 56:431–443.

Kerminen, V. M., Pirjola, L., Boy, M., Eskola, A., Teinnila, K., Laakso, L., Asmi, A., Hienola, J., Lauri, A., Vainio, V., Lehtinen, K., and Kulmala, M. (2000). Interaction between SO_2 and Submicron Atmospheric Particles, *Atmos. Environ.* 52:41–57.

Kim, E., Hopke, P. K., and Edgerton, E. S. (2003). Source Identification of Atlanta Aerosol Using Positive Matrix Factorization, *J. Air and Waste Manage. Assoc.* 53:731–739.

Kim, E., Hopke, P. K., Larson, T. V., and Covert, D. S. (2004). Analysis of Ambient Particle Size Distributions Using UNMIX and Positive Matrix Factorization, *Environ. Sci. Technol.* 38:202– 209.

Kleeman, M. J., Schauer, J. J., and Cass, G. (1999). Size and Composition Distribution of Fine Particulate Matter Emitted from Wood Burning, Meat Charbroiling, and Cigarettes, *Environ. Sci. Technol.* 33:3516–3523.

Laden, F., Neas, L. M., Dockery, D. W., and Schwartz, J. (2000). Association of Fine Particulate Matter from Different Sources with Daily Mortality in six US Cities, *Environ. Health Perspect.* 108:941–947.

Lee, E., Chan, C. K., and Paatero, P. (1999). Application of Positive Matrix Factorization in Source Apportionment of Particulate Pollutants in Hong Kong, *Atmos. Environ.* 33:3201–3212.

Li, Z., Hopke, P. K., Husain, L., Qureshi, S., Dutkiewicz, V. A., Schwab, J. J., Drewnick, F., and Demerjian, K. L., 2004. Sources of Fine Particle Composition in New York City, *Atmos. Environ.* 38:6521–6529.

Linak, W. P., Miller, C. A., and Wendt, J. O. L. (2000). Comparison of Particle Size Distributions and Elemental Partitioning from the Combustion of Pulverized Coal and Residual Fuel oil, *J. Air & Waste Manage. Assoc.* 50:1532–1544.

Maguhn, J., Karg, E., Kettrup, A., and Zimmermann, R. (2003). On-line Analysis of the Size Distribution of Dine and Ultrafine Aerosol Particles in Flue and Stack Gas of a Municipal Waste Incineration Plant: Effects of Dynamic Process Control Measures and Emission Reduction Devices, *Environ. Sci. Technol.* 37:4761–4770.

Miller, C. A., Linak, W. P., King, C., and Wendt, J. O. L. (1998). Fine Particle Emissions From Heavy Fuel Oil Combustion in a Firetube Package Boiler, *Combust. Sci. Technol.* 134:477–502.

Morawska, L., Thomas, S., Bofinger, N., Wainwright, D., and Neale, D. (1998). Comprehensive Characterization of Aerosols in a Subtropical Urban Atmosphere: Particle Size Distribution and Correlation with Gaseous Pollutants, *Atmos. Environ.* 32:2467–2478.

Morawska, L., Johnson, G. R., He, C., Ayoko, G. A., Lim, M. C. H., Swanson, C., Ristovski, D., and Moore, M. (2006). Particle Number Emissions and Source Signatures of an Industrial Facility, *Environ. Sci. Technol.* 40:803–814.

Moya, M., Ansari, A., and Pandis, S. N. (2001). Partitioning of Nitrate and Ammonium Between the Gas and Particulate Phases During the 1997 IMADAAVER Study in Mexico City, *Atmos. Environ.* 35:1791–1804.

Nygaard, U. C., Samuelsen, M., Aase, A., and Løvik, M. (2004). The Capacity of Particles to Increase Allergic Sensitization Is Predicted by Particle Number and Surface Area, Not by Particle Mass, *Toxicol. Sci.* 82:515–524.

Oberdörster, G., Gelein, R., Ferin, J., and Weiss, B. (1995). Association of Particulate Air Pollution and Acute Mortality: Involvement of Ultrafine Particles? *Inhal. Toxicol.* 7:111–124.

Ogulei, D., Hopke, P. K., and Wallace, L. A. (2006a). Analysis of Indoor Particle Size Distributions From an Occupied Townhouse Using Positive Matrix Factorization, *Indoor Air* 16:204–215.

Ogulei, D., Hopke, P. K., Zhou, L., Pancras, J. P., Nair, N., and Ondov, J. M. (2006b). Source Apportionment of Baltimore Aerosol From Combined Size Distribution and Chemical Composition Data, *Atmos. Environ.* 40:S396–S410.

Paatero, P. (1997). Least Squares Formulation of Robust Non-Negative Factor Analysis. *Chemom. Intell. Lab. Syst.* 37:23–35.

Paatero, P., Hopke, P. K., Song, X. H., and Ramadan, Z. (2002). Understanding and Controlling Rotations in Factor Analytic Models, *Chemom. Intell. Lab. Syst.* 60:253–264.

Pekkanen, J., Timonen, K.L., Ruuskanen, J., Reponen, A., and Mirme, A. (1997). Effects of Ultra-Fine and Fine Particles in Urban Air on Peak Expiratory Flow Among Children with Asthmatic Symptoms, *Environ. Res.* 74:24–33.

Penn, A., Murphy, G., Barker, S., Henk, W., and Penn, L. (2005). Combustion-Derived Ultrafine Particles Transport Organic Toxicants to Target Respiratory Cells, *Environ. Health Perspect.* 113:956–963.

Peters, A., Wichmann, H. E., Tuch, T., Heinrich, J., and Heyder, J. (1997). Respiratory Effects are Associated with the Number of Ultrafine Particles, *Am. J. Respir. Crit. Care Med.* 155:1376–1383.

Qin,Y., Oduyemi, K., and Chan, L. Y. (2002). Comparative Testing of PMF and CFA Models, *Chemom. Intell. Lab. Syst.* 61:75–87.

Rattigan, O. V., Hogrefe, O., Felton, H. D., Schwab, J. J., Roychowdhury, U. K., Husain, L., Dutkiewicz, V. A., and Demerjian, K. L. (2006). Multi-year Urban and Rural Semi-Continuous $PM_{2.5}$ Sulfate and Nitrate Measurements in

New York State: Evaluation and Comparison with Filter Based Measurements, *Atmos. Environ.* 40:S192–S205.

Ristovski, Z. D., Morawska, L., Bofinger, N. D., and Hitchins, J. (1998). Submicrometer and Supermicrometer Particles from Spark Ignition Vehicles, *Environ. Sci. Technol.* 32:3845–3852.

Rosenbohm, E., Vogt, R., Scheer, V., Nielsen, O. J., Dreiseidler, A., Baumbach, G., Imhof, D., Baltensperger, U., Fuchs, J., and Jaeschke, W. (2005). Particulate Size Distributions and Mass Measured at a Motorway During the BAB II Campaign, *Atmos. Environ.* 39:5696–5709.

Seaton, A., MacNee, W., Donaldson, K., and Godden, D. (1995). Particulate Air Pollution and Acute Health Effects, *Lancet* 345:176–178.

Seinfeld, J. H., and Pandis, S. N. (1998). *Atmospheric Chemistry and Physics: From Air Pollution to Climate Change*. John Wiley and Sons, New York, p. 531–539.

Shi, J. P., and Harrison, R. M. (1999). Investigation of Ultrafine Particle Formation During Diesel Exhaust Dilution, *Environ. Sci. Technol.* 33:3730–3736.

Sioutas, C., Delfino, R. J., and Singh, M. (2005). Exposure Assessment for Atmospheric Ultrafine Particles (UFPs) and Implications in Epidemiologic Research, *Environ. Health Perspect.* 113:947–955.

Song, X. H., Polissar, A. V., and Hopke, P.K. (2001). Sources of Fine Particle Composition in the Northeastern US, *Atmos. Environ.* 35:5277–5286.

Song, Y., Zhang, Y., Xie, S., Zeng, L., Zheng, M., Salmon, L. G., Shao, M., and Slanina, S. (2006). Source Apportionment of $PM_{2.5}$ in Beijing by Positive Matrix Factorization, *Atmos. Environ.* 40:1526–1537.

Stelson, A. W., and Seinfeld, J. H. (1982). Relative Humidity and Temperature Dependence of the Ammonium Nitrate Dissociation Constant, *Atmos. Environ.* 16:983–992.

Tang, I. N., and Munkelwitz, H. R. (1993). Composition and Temperature Dependence of the Deliquescence Properties of Hygroscopic Aerosols, *Atmos. Environ.* 27A:467–473.

Tolocka, M. P., Lake, D. A., Johnston, M. V., and Wexler, A. S. (2004). Ultra Fine Nitrate Particle Events in Baltimore Observed by Real-Time Single Particle Mass Spectrometry, *Atmos. Environ.* 38:3215–3223.

Wichmann, H. E., Spix, C., Tuch, T., Wolke, G., Peters, A., Herinrich, J., Kreyling, W. G., and Heyder, J. (2000). Daily Mortality and Fine and Ultrafine Particles in Erfurt, Germany, Part A: Role of Particle Number and Particle Mass, *Health Effects Institute Research Report 98*.

Wittig, A.E., Takahama, S., Khlystov, A. Y., Pandis, S. N., Hering, S., Kirby, B., and Davidson, C. (2004). Semi-continuous $PM_{2.5}$ Inorganic Composition Measurements During the Pittsburgh Air Quality Study, *Atmos. Environ.* 38:3201–3213.

Zhang, K. M., Wexler, A. S., Zhu, Y. F., Hinds, W. C., and Sioutas, C. (2004). Evolution of Particle Number Distribution Near Roadways. Part II: the 'Road-to-Ambient' Process, *Atmos. Environ.* 38:6655–6665.

Zhou, L., Kim, E., Hopke, P. K., Stanier, C., and Pandis S. N. (2005a). Mining Airborne Particulate Size Distribution Data by Positive Matrix Factorization, *J. Geophys. Res.* 110:D07S19, doi:10.1029/2004JD004707.

Zhou, L., Hopke, P. K., Stanier, C. O., Pandis, S. N., Ondov, J. M., and Pancras, J.P. (2005b). Investigation of the Relationship Between Chemical Composition and size Distribution of Airborne Particles by Partial Least Squares (PLS) and Positive Matrix Factorization (PMF), *J. Geophys. Res.* 110, doi:10.1029/2004JD005050.

Zhuang, H., Chan, C. K., Fang, M., and Wexler, A. S. (1999). Size Distributions of Particulate Sulfate, Nitrate, and Ammonium at a Coastal site in Hong Kong, *Atmos. Environ.* 33:843–853.

SUPPLEMENTARY MATERIAL

Table S1 shows the instruments used for acquiring the data employed in this study. Figure S1 shows a plot of the sum of squares, Q, as a function of the rotation parameter, FPEAK, for winter, spring, and summer data sets. Figures S2 to S5 are 24-hour spatial plots of the raw 5-minutes data measured by the SMPS used in this study. The color scale shows the logarithm of the number concentrations for each size bin (N_p in #/cm^3; 5 minutes measurements). The highest concentrations are represented by the hottest color. Figures S6 and S7 show the particle volume profiles of all the resolved sources.

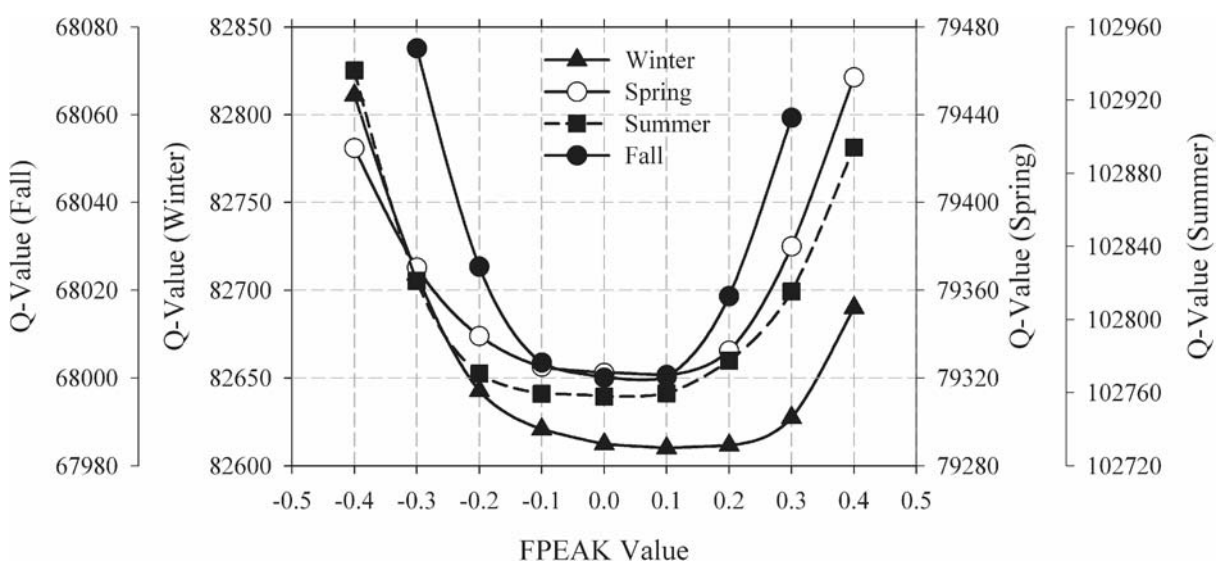

Figure S1. Plot of Q as a function of FPEAK for winter, spring, summer, and fall data sets.

Table S1
Instruments used for acquiring the data employed in this study. Particle size measurements were made every five minutes while other parameters were measured hourly

Species/Parameter	Experimental Method	Instrument/Model
Particle Size (0.011–0.470 (μm, logarithmically spaced)	Particle sizing	SMPS^{TM} model 3034, Electrostatic classifer model 3071, DMA model 3081, ^{85}Kr aerosol neutralizer model 3077, CPC model 3010 (TSI Inc., Shoreview, MN)
CO	Non-dispersive infrared light absorption. Utilizes Gas Filter Correlation (GFC)	Thermo Electron (TECO) Model 48C (Thermo Electron Corporation, Waltham, MA)
SO_2	Pulsed Fluorescence	TECO Model 43C
O_3	Ultraviolet light absorption (UV Photometer with internal calibrator)	TECO Model 49C
$PM_{2.5}$	Direct measurement of $PM_{2.5}$ mass in sample	Tapered Element Oscillating Microbalance (TEOM) R&P Model 1400AB (Rupprecht and Patashnick, Albany, NY)
Wind Direction	Arithmetic average and resultant wind direction	Met One Model 50.5h heated ultrasonic wind speed/wind direction sensor (Met One Instruments, Grants Pass, OR)
Wind Speed	Arithmetic average and resultant wind speed	Same as for Wind Direction
Temperature	Direct measurement of ambient temperature	NovaLynx Model 225-503, -40 to +140 °F, 0 to 100 %. Temperature and Relative Humidity Sensor (NovaLynx Corp., Auburn, CA).
Relative Humidity (RH)	Direct measurement of ambient RH	Same as for Temperature
Barometric Pressure (BP)	Direct measurement of pressure.	NovaLynx Model 230-276-8, 800-1100 mb pressure range.

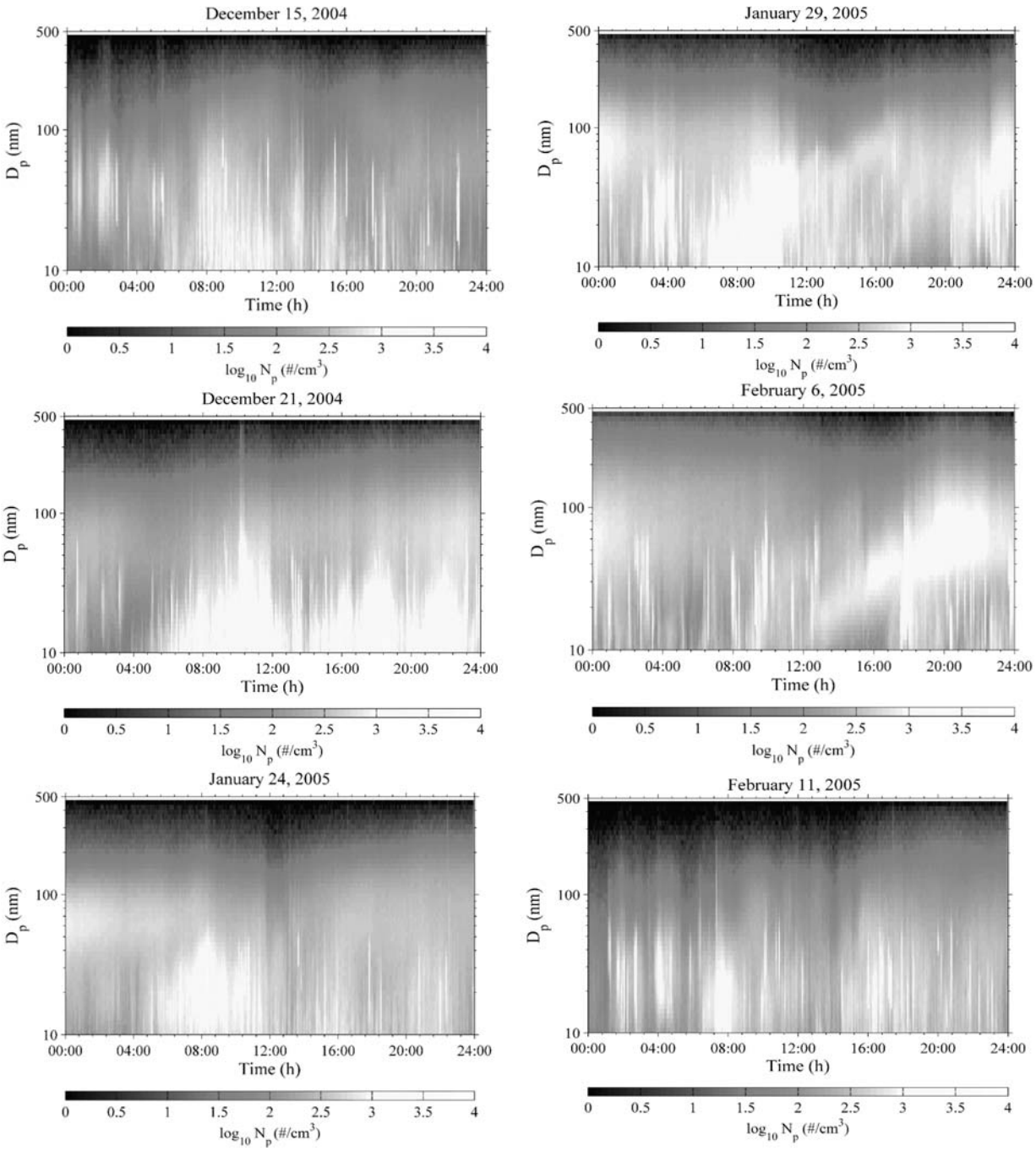

Figure S2. Sample spatial plots for winter.

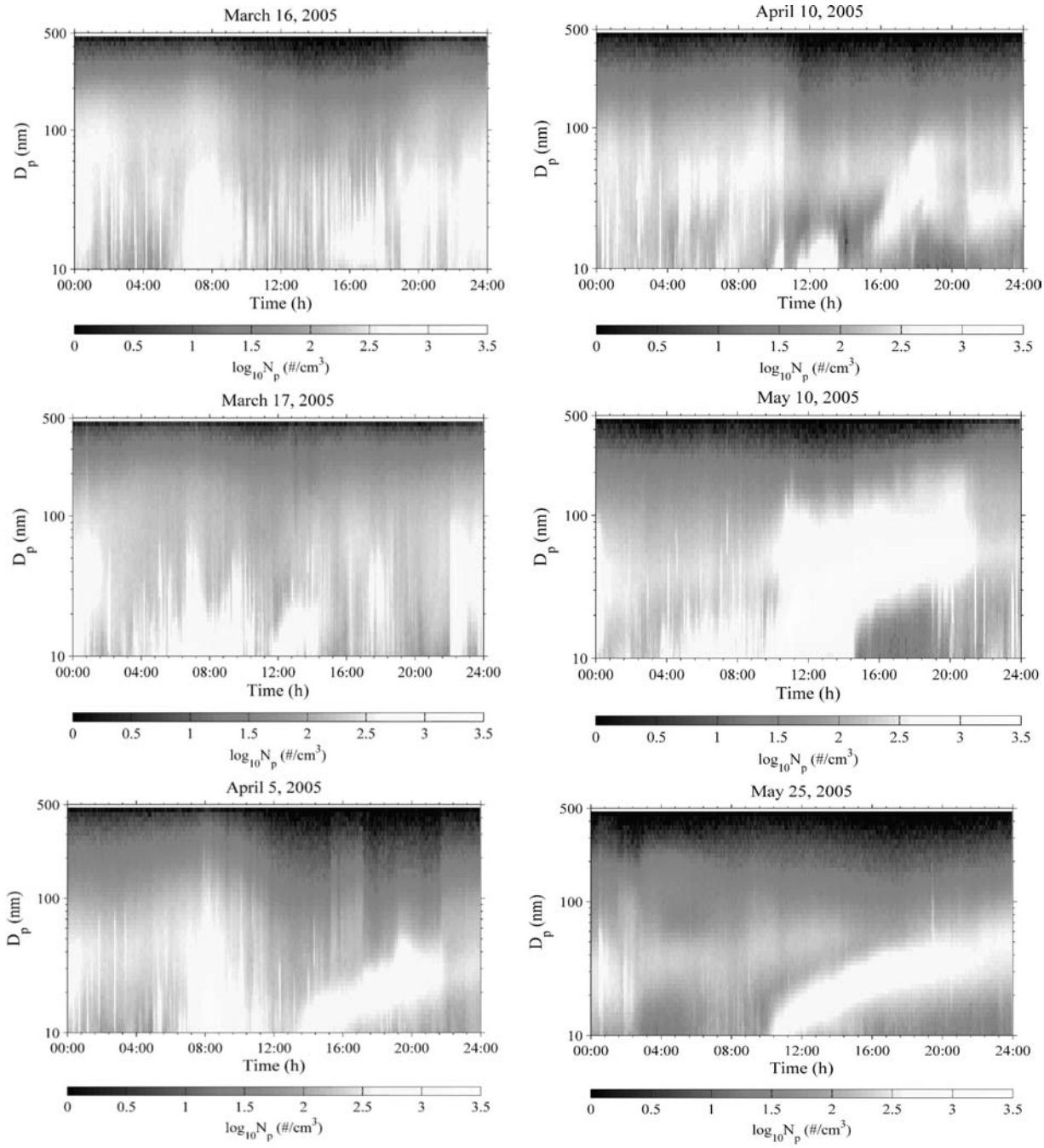

Figure S3. Sample spatial plots for spring.

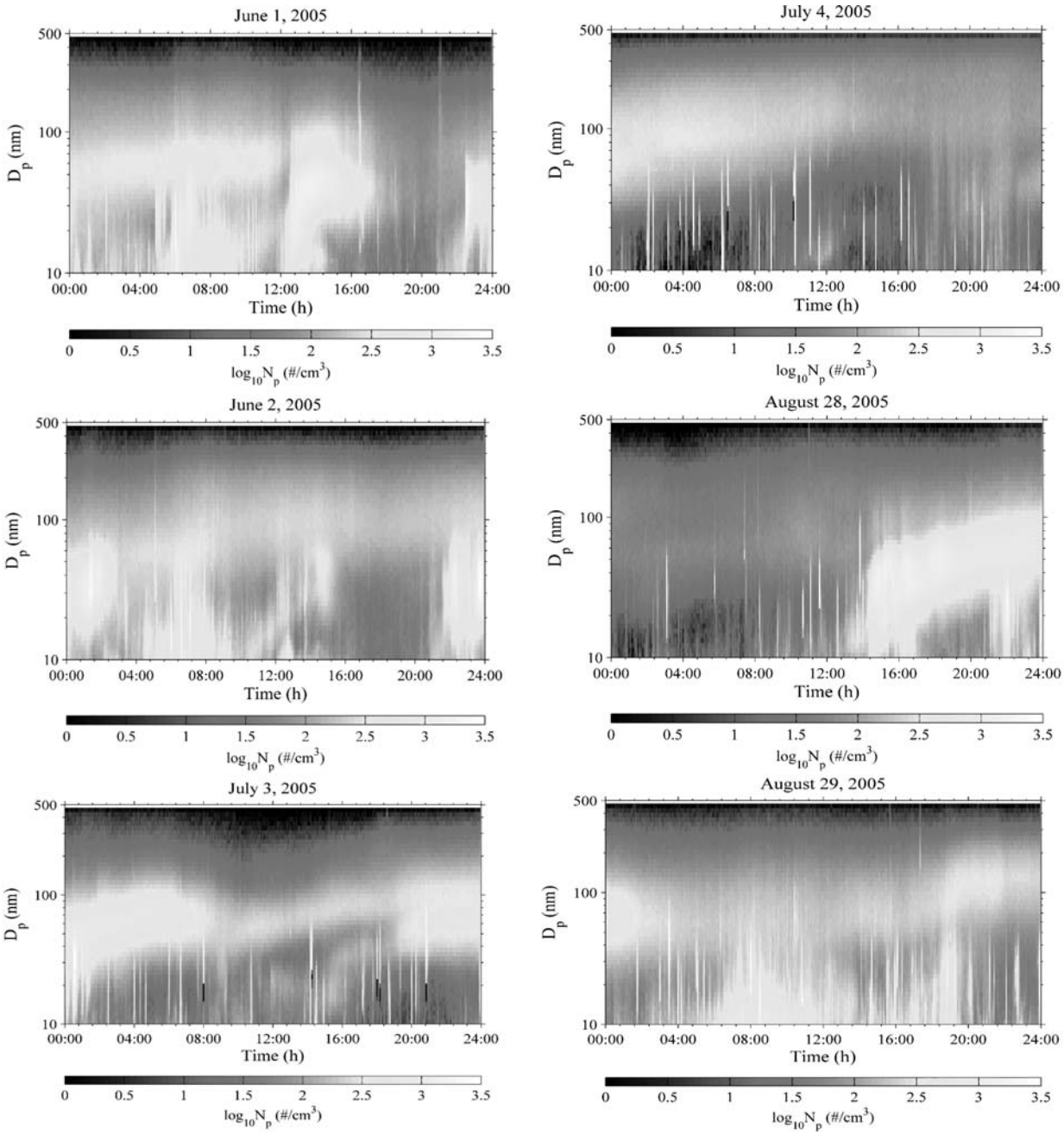

Figure S4. Sample spatial plots for summer.

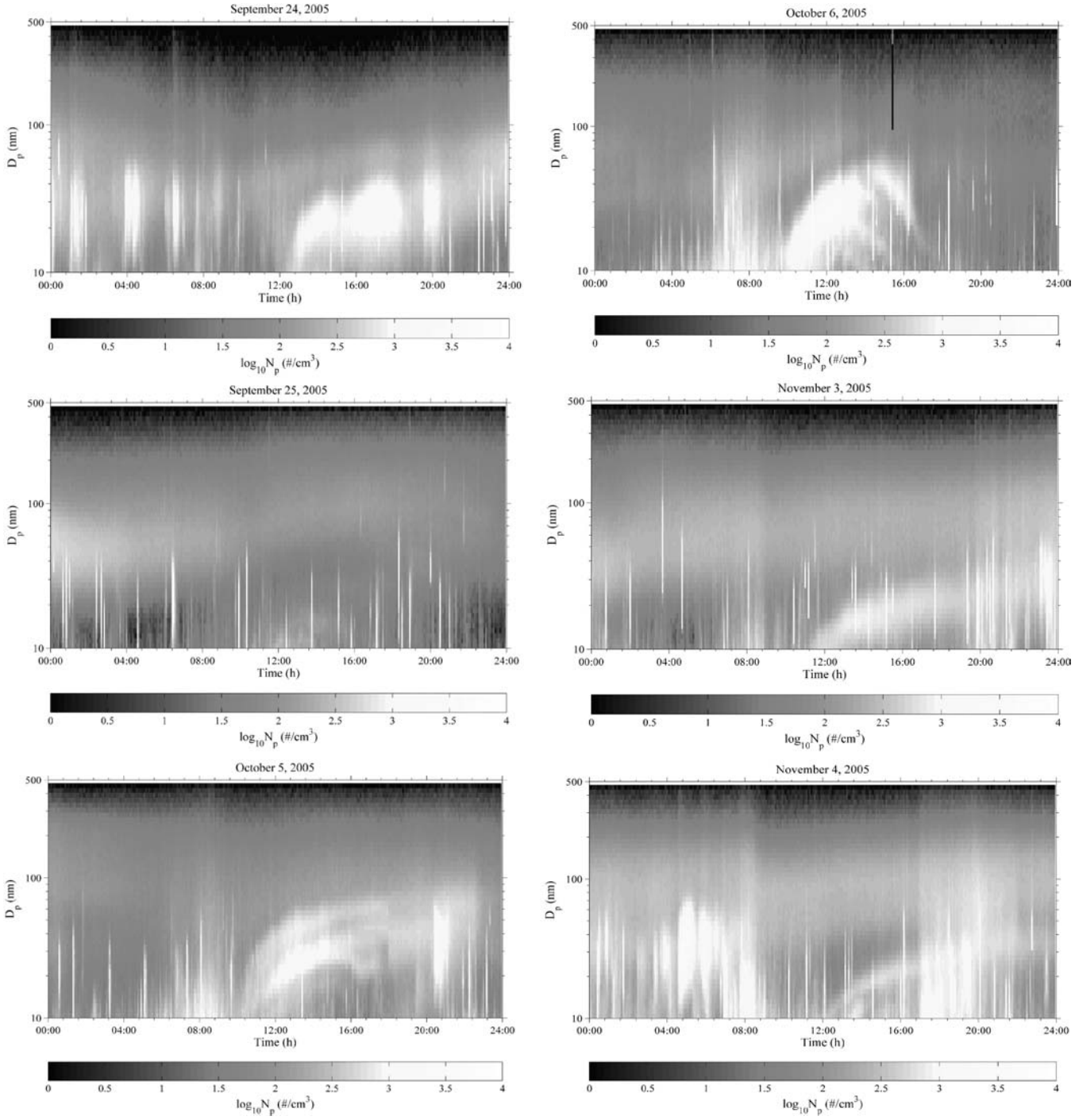

Figure S5. Sample spatial plots for fall.

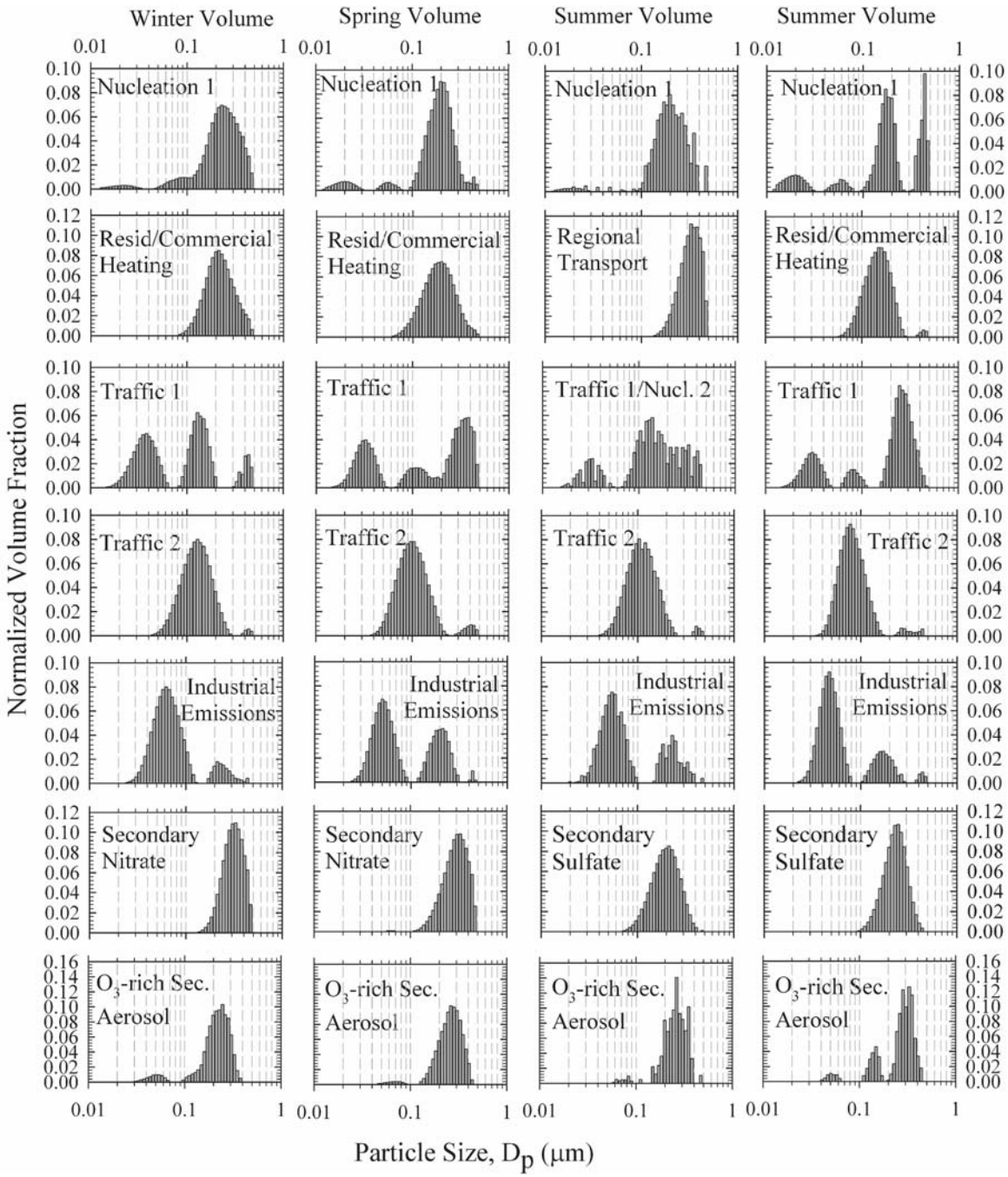

Figure S6. Volume profiles of all the sources.

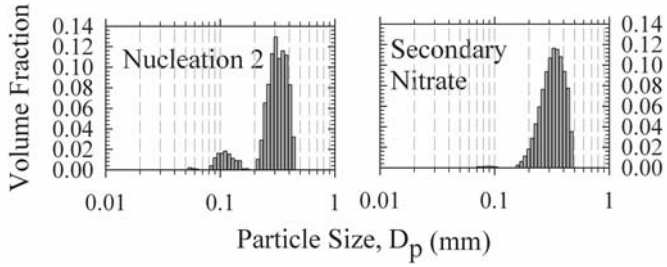

Figure S7. Volume profiles for the fall factors.